Environmental Persistence and Threshold Dynamics in a Multi-Region Cholera Model

Original Research Article

Abstract

Cholera remains a major global health concern, particularly in regions with limited sanitation and high population mobility. Motivated by the 2010 Haiti earthquake and subsequent outbreak, this study examines the roles of environmental reservoirs, and spatial coupling in cholera transmission, using a coupled SEIR-B and hydrodynamic modeling framework. Human disease dynamics are integrated with environmental bacterial transport via advection and diffusion, together with cross-regional coupling mechanisms. Analysis of the basic reproduction number $\mathcal{R}_0$, stability properties, and numerical simulations identifies thresholds separating bacterial elimination from persistence and demonstrates how hydrological transport, exogenous contamination, and upstream sources shape downstream risk. Numerical results further show even localized external contamination can sustain downstream bacterial persistence despite local control of human infections. These results underscore the need for coordinated sanitation and water-management interventions in hydrologically connected regions. They also highlight the importance of region-level coordination when designing effective cholera control strategies.

Keywords: cholera; waterborne transmission; environmental diffusion; exogenous contamination; PDE epidemiology; $\mathcal{R}_0$; global stability.

2010 Mathematics Subject Classification: 53C25; 83C05; 57N16

1 Introduction

Cholera is an acute, waterborne infectious disease caused by the bacterium *Vibrio cholerae*, transmitted primarily through ingestion of contaminated water or food. Clinical outcomes range from mild diarrhea to severe dehydration and shock, and without prompt re-hydration therapy, death may occur within hours. Because *V. cholerae* proliferates in aquatic environments, particularly in regions with inadequate drinking water and sanitation, cholera transmission is closely linked to environmental

conditions and population exposure to contaminated water sources (World Health Organization, 2024; Médecins Sans Frontières, 2024; Centers for Disease Control and Prevention, 2024a,b).

Unlike many directly transmitted diseases, cholera outbreaks are frequently sustained by persistent environmental reservoirs in rivers, wells, and community water systems rather than by person-to-person contact alone. These mechanisms have motivated mathematical models incorporating diffusion, advection, and spatial heterogeneity through partial differential equations (Cai et al., 2016; Gobbert and Agheksanterian, 2007; Jung et al., 2016; Shu et al., 2021a; Yamazaki and Wang, 2017; Shu et al., 2021b; Rosa and Torres, 2021). Because environmental contamination can persist long after clinical cases decline, sustaining transmission and enabling re-emergence, understanding how water movement, infrastructure failure, and sanitation influence bacterial persistence is essential for accurate modeling and effective intervention design.

Haiti provides a particularly instructive case study for environmentally driven cholera transmission. The 2010 epidemic began when *Vibrio cholerae* was introduced into the Artibonite River near Mirebalais, after which contaminated water spread rapidly downstream to communities such as Gonaïves that rely on the river for drinking and agriculture. Seasonal rainfall, flooding, and watershed flow amplified bacterial transport. This underscored the central role of aquatic forcing in cholera persistence and re-emergence.

Structural vulnerabilities further magnified these dynamics. Limited sanitation infrastructure, high population density in urban centers such as Port-au-Prince, and constrained medical capacity influenced both transmission intensity and the timing of interventions. These conditions make Haiti well suited for mechanistic models that couple human epidemiological dynamics with environmental bacterial transport via diffusion and advection (Cai et al., 2016; Gobbert and Agheksanterian, 2007; Jung et al., 2016; Shu et al., 2021a; Yamazaki and Wang, 2017; Shu et al., 2021b; Rosa and Torres, 2021).

Despite extensive public health responses, (including surveillance, treatment, and vaccination campaigns implemented by the MSPP, WHO, PAHO, UNICEF, CDC, and Médecins Sans Frontières) environmental contamination persisted long after reported cases declined, highlighting the need for models that explicitly capture bacterial survival in aquatic reservoirs and drivers of sustained transmission (World Health Organization, 2024; Médecins Sans Frontières, 2024; Centers for Disease Control and Prevention, 2024a,b).

Represented here by the parameter Λ_i, exogenous contamination captures bacterial inputs originating outside the local human-environment system. In 2010, improper disposal of human waste by UN peacekeepers near the Mirebalais base resulted in the direct release of contaminated sewage into the Artibonite River, abruptly initiating widespread downstream transmission. Mathematically, Λ_i enters the environmental compartment as an external source term independent of local human shedding. When combined with hydrological transport, diffusion, and flood-season dynamics, such inputs can generate nonlinear amplification effects and sustain bacterial persistence (Cai et al., 2016; Gobbert and Agheksanterian, 2007; Jung et al., 2016; Shu et al., 2021a; Yamazaki and Wang, 2017; Shu et al., 2021b; Rosa and Torres, 2021).

Recent work in epidemic modeling has explored stability, bifurcation, and threshold phenomena using a variety of mathematical frameworks, including fractional-order formulations and perturbation-based methods (Owoyemi et al., 2022, 2021, 2025). Although these approaches differ from the integer-order SEIR-B framework considered here, they offer complementary perspectives on persistence and control thresholds, that motivate continued investigation of structurally driven epidemic dynamics.

In the context of cholera, a substantial body of work has emphasized the role of environmental drivers, aquatic processes, and intervention strategies in shaping persistence and control, particularly in communities linked by flowing water systems like Haiti (Finger et al., 2016; Azman et al., 2016; Weill et al., 2017). More recent studies further highlight the sustained global burden of cholera and the increasing influence of environmental and climatic factors on disease persistence, underscoring the need for coordinated, region-level intervention strategies (Ali et al., 2020; Lessler et al., 2021; Qadri et al., 2023).

Despite these advances, the mathematical modeling literature leaves room for further development. While many existing cholera models incorporate spatial structure or environmental transmission, few frameworks explicitly represent seasonally varying diffusion despite strong empirical evidence linking rainfall and flooding to bacterial transport. Even fewer models include exogenous environmental forcing, despite documented outbreaks in which external contamination dominates local transmission dynamics. Moreover, although prior studies establish threshold and stability results (Cai et al., 2016; Gobbert and Agheksanterian, 2007; Jung et al., 2016; Shu et al., 2021a; Yamazaki and Wang, 2017; Shu et al., 2021b; Rosa and Torres, 2021), few derive analytical persistence conditions that simultaneously account for spatial heterogeneity, aquatic variability, and external environmental inputs.

To contribute to the mathematical modeling literature, we develop a coupled ODE-PDE framework in which human disease dynamics are governed by ODEs and environmental *V. cholerae* concentrations evolve according to a PDE with seasonally varying diffusion and explicit exogenous forcing. Section 2 introduces the resulting multi-region SEIR–B model, and Section 3.1 establishes its well-posedness. Within this framework, we analyze the basic reproduction number $\mathcal{R}_0$ and derive conditions for global asymptotic stability of the disease-free equilibrium in Section 3, identifying an environmental persistence threshold that reflects the combined effects of water-driven connectivity and exogenous inputs. Section 4 presents numerical simulations illustrating how outbreaks may be initiated, sustained, and propagated across connected regions, and Section 5 discusses the resulting epidemiological and policy implications.

2 Model Formulation

2.1 Visualization and Narrative Overview of the Model

We first present a schematic representation of the population compartments and their interactions, followed by the governing equations describing disease progression, bacterial transport, and inter-regional coupling. This framework builds on classical compartmental epidemic theory and cholera-specific extensions incorporating environmental reservoirs (Hethcote, 2000; Anderson and May, 1991; Kermack and McKendrick, 1927; Codeço, 2001). Figure 1 depicts transitions among susceptible (S_i), exposed (E_i), infectious (I_i), and recovered (R_i) compartments across multiple regions, driven by direct transmission, environmental exposure, disease progression, and demographic processes.

Figure 1: Flowchart of the 3–Region SEIR–B Cholera Model.

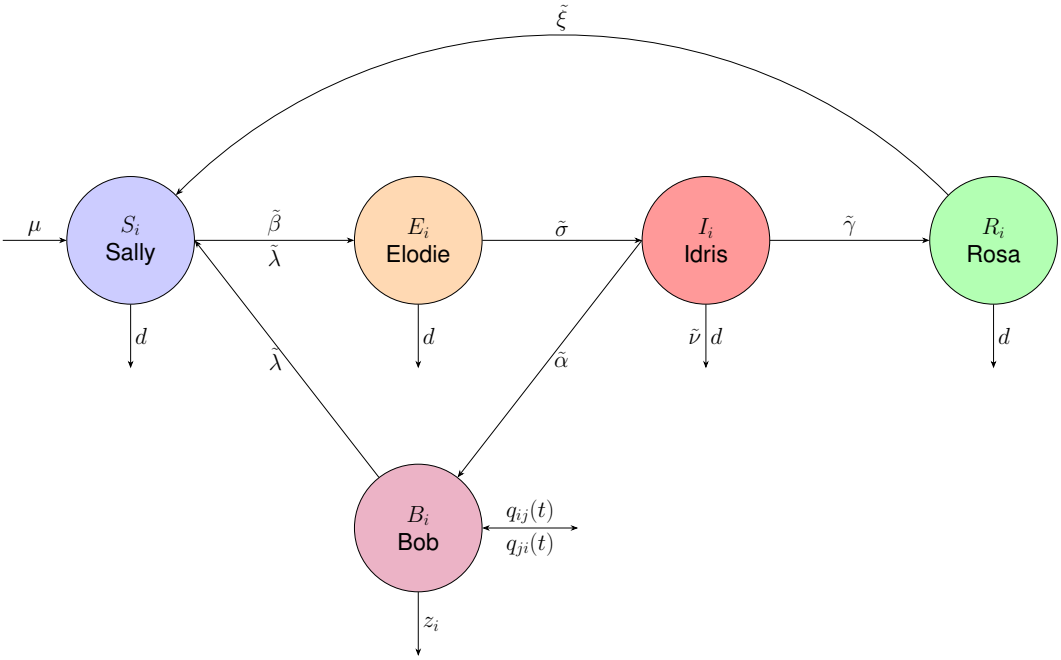

Within each region i, human disease dynamics are linked to an environmental reservoir of waterborne *Vibrio cholerae*. Susceptible individuals enter through recruitment at rate μ or loss of immunity at rate $\tilde{\xi}R_i$. Infection occurs via direct contact with infectious individuals at rate $\tilde{\beta}\frac{I_i}{N_i}S_i$ (Kermack and McKendrick, 1927) or environmental exposure to contaminated water at rate $\tilde{\eta}\frac{B_i}{K+B_i}S_i$ (Codeço, 2001).

Exposed individuals represent a latent stage and progress to infectiousness at rate $\tilde{\sigma}E_i$, while all human compartments experience natural mortality at rate d (Hethcote, 2000). Infectious individuals recover at rate $\tilde{\gamma}I_i$, experience disease-induced mortality at rate $\tilde{\nu}I_i$, and shed bacteria into the environment at rate $\tilde{\alpha}I_i$ (Codeço, 2001). Immunity following recovery is temporary and wanes at rate $\tilde{\xi}R_i$ (Anderson and May, 1991).

Environmental bacteria evolve according to an advection-diffusion-reaction equation. Transport is governed by hydrological advection with velocity $\mathbf{v}_i$ and diffusion with coefficient D_i, capturing directed flow and local mixing in riverine systems (Tien and Earn, 2010; Bertuzzo et al., 2010). Bacterial inputs arise from human shedding, while removal occurs at rate z_iB_i, reflecting natural decay and sanitation-related processes (Hartley et al., 2006; King et al., 2008). Inter-regional coupling is modeled through time-dependent transport terms $q_{ij}(t)$, representing hydrological export and upstream inflow (Bertuzzo et al., 2010). Exogenous contamination is incorporated via $\Lambda_i(t)$, capturing external inputs such as flooding, runoff, or infrastructure failure (Mari et al., 2012; Chin et al., 2011).

Although bacterial transport is inherently three-dimensional, we adopt a depth-averaged 2-D formulation appropriate for rivers, floodplains, and shallow surface waters in cholera-endemic regions. Vertical mixing driven by turbulence, suspended particulates, and flood-season hydrodynamics

justifies this approximation while reducing computational complexity (Huq and et al., 1983; Colwell and et al., 2003; King et al., 2008; Hartley et al., 2006; Bertuzzo et al., 2010).

This SEIR-B structure enables systematic evaluation of sanitation, vaccination, and water-based intervention strategies in interconnected regions (Zhu et al., 2023; Iyaniwura et al., 2023; Wang et al., 2022). Model parameters are summarized in Table 1.

2.2 Mathematical Model Formulation

The SEIR system is defined as follows:

$$\begin{aligned}
\frac{dS_i}{dt} &= \mu + \tilde{\xi} R_i - \tilde{\beta} \frac{I_i}{N_i} S_i - \tilde{\eta} \frac{B_i}{K + B_i} S_i - d S_i, \\
\frac{dE_i}{dt} &= \tilde{\beta} \frac{I_i}{N_i} S_i + \tilde{\eta} \frac{B_i}{K + B_i} S_i - \tilde{\sigma} E_i - d E_i + \Pi_i(t), \\
\frac{dI_i}{dt} &= \tilde{\sigma} E_i - \tilde{\gamma} I_i - \tilde{\nu} I_i - d I_i, \\
\frac{dR_i}{dt} &= \tilde{\gamma} I_i - \tilde{\xi} R_i - d R_i.
\end{aligned} \tag{2.1}$$

Environmental bacterial concentration in region i evolves according to:

$$\frac{\partial B_i}{\partial t} + \mathbf{v}_i \cdot \nabla B_i = D_i \nabla^2 B_i + \tilde{\alpha}\, I_i + \sum_{j \neq i} q_{ji}(t)\, B_j - \sum_{j \neq i} q_{ij}(t)\, B_i - z_i B_i + \Lambda_i(t), \qquad i \in \{1, 2, 3\}. \tag{2.2}$$

Table 1: **Model Variables and Parameters with Embedded Vaccination Effects**

Symbol	Description
i	Region index, $i \in \{1, 2, 3\}$.
$S_i(t)$	Susceptible population in region i
$E_i(t)$	Exposed population in region i
$I_i(t)$	Infectious population in region i
$R_i(t)$	Recovered population in region i
$N_i(t)$	Total population in region i; $N_i(t) = S_i(t) + E_i(t) + I_i(t) + R_i(t)$
$B_i(x, t)$	Environmental bacterial concentration in region i at location x and time t
K	Half-saturation constant for environmental transmission
μ	Birth/Recruitment rate.
d	Natural death rate
$\tilde{\beta} = \beta(1 - \epsilon_S)$	Human-to-human transmission rate accounting for reduced susceptibility.

$\tilde{\eta} = \eta(1 - \epsilon_B)$	Environment-to-human transmission rate modified by interventions limiting exposure.
$\tilde{\sigma} = \sigma(1 - \epsilon_E)$	Progression rate from exposed to infectious modified by intervention effects.
$\tilde{\gamma} = \gamma(1 + \epsilon_I)$	Recovery rate modified by intervention effects.
$\tilde{\nu} = \nu(1 - \epsilon_I)$	Disease-induced mortality rate modified by interventions.
$\tilde{\xi} = \xi(1 - \epsilon_R)$	Immunity waning rate modified by interventions.
$\tilde{\alpha} = \alpha(1 - \epsilon)$	Bacterial shedding rate modified by interventions.
$\mathbf{v}_i$	Advection (velocity) vector representing directional water flow in region i
D_i	Diffusion coefficient for bacterial spread within region i.
$q_{ij}(t) := a_{ji}\, r_{ij}(t)$	Time-dependent bacterial transport rate from region i to region j.
a_{ij}	Binary hydrological connectivity indicator between regions i and j.
$r_{ij}(t)$	Time-dependent runoff-driven transport intensity from region i to region j
z_i	Net bacterial removal rate in region i
$\Lambda_i(t)$	Local external bacterial input in region i

2.3 Model Structure and Assumptions

The SEIR-B cholera transmission model (2.1) is formulated under the following biological, environmental, and structural assumptions:

1. **Homogeneous mixing within regions.** Within each region i, individuals mix uniformly. Susceptible individuals experience equal contact with infectious individuals and equal exposure to environmental bacteria. No within-region heterogeneity (e.g., age or behavior) is represented.
2. **Deterministic compartmental dynamics.** Human populations evolve according to deterministic ODEs, and environmental bacteria evolve according to deterministic advection-diffusion PDEs, representing mean-field dynamics. Stochastic effects are neglected.
3. **Interventions act through rate modification.** Public health interventions are modeled via scaling parameters $\epsilon_S, \epsilon_B, \epsilon_E, \epsilon_I$, and ϵ_R, modifying susceptibility, environmental exposure, disease progression, severity, and immunity duration.
4. **Saturating environmental transmission.** Environmental transmission follows a Michaelis-Menten-type response $B_i/(K + B_i)$, reflecting saturation of infection risk at high bacterial concentrations.
5. **Population turnover without explicit human mobility.** Regional populations change only through recruitment μ and natural or disease-induced mortality d. Human migration between regions is not explicitly modeled in the SEIR compartments.
6. **Latent infection and temporary immunity.** Exposed individuals are infected but not infectious and progress to the infectious class at rate $\tilde{\sigma}$. Immunity following recovery is temporary and wanes at rate $\tilde{\xi}$.
7. **Uniform natural mortality and no reinfection during infection.** All human compartments experience the same natural death rate d, and reinfection does not occur during the exposed or infectious stages.

8. **Environmental bacteria as the sole indirect transmission pathway.** Waterborne *Vibrio cholerae* constitutes the only environmental reservoir. No alternative indirect transmission routes are considered.

9. **Advection-diffusion-reaction environmental dynamics.** Environmental bacteria evolve via advection, diffusion, shedding from infectious individuals, hydrological transport $q_{ij}(t)$, linear removal at rate $z_i B_i$, and exogenous input $\Lambda_i(t)$. No latent or persistent bacterial states are modeled.

10. **No healthcare capacity or behavioral feedback.** Rates of recovery, mortality, and treatment effectiveness are assumed constant and independent of disease prevalence (Hethcote, 2000).

11. **Region-specific importation, hydrology, and forcing.** Human-mediated importation occurs only into Port-au-Prince: $\Pi_1 = \Pi_2 = 0$, $\Pi_3 = m_{13} I_1 + m_{23} I_2$. Waterways connect Mirebalais (Region 1) to Gonaïves (Region 2), while Port-au-Prince (Region 3) is hydrologically isolated. External environmental forcing occurs only in Mirebalais, with $\Lambda_1 \neq 0$ and $\Lambda_2 = \Lambda_3 = 0$.

Updated model incorporating assumptions:

$$
\begin{aligned}
\frac{dS_1}{dt} &= \mu + \tilde{\xi}R_1 - \tilde{\beta}\frac{I_1}{N_1}S_1 - \tilde{\eta}\frac{B_1}{K+B_1}S_1 - dS_1,\\
\frac{dE_1}{dt} &= \tilde{\beta}\frac{I_1}{N_1}S_1 + \tilde{\eta}\frac{B_1}{K+B_1}S_1 - \tilde{\sigma}E_1 - dE_1,\\
\frac{dI_1}{dt} &= \tilde{\sigma}E_1 - \tilde{\gamma}I_1 - \tilde{\nu}I_1 - dI_1,\\
\frac{dR_1}{dt} &= \tilde{\gamma}I_1 - \tilde{\xi}R_1 - dR_1,\\
\frac{\partial B_1}{\partial t} + \mathbf{v}_1\cdot\nabla B_1 &= D_1\nabla^2 B_1 + \tilde{\alpha}I_1 - q_{12}(t)B_1 - z_1B_1 + \Lambda_1(t),\\
\frac{dS_2}{dt} &= \mu + \tilde{\xi}R_2 - \tilde{\beta}\frac{I_2}{N_2}S_2 - \tilde{\eta}\frac{B_2}{K+B_2}S_2 - dS_2,\\
\frac{dE_2}{dt} &= \tilde{\beta}\frac{I_2}{N_2}S_2 + \tilde{\eta}\frac{B_2}{K+B_2}S_2 - \tilde{\sigma}E_2 - dE_2,\\
\frac{dI_2}{dt} &= \tilde{\sigma}E_2 - \tilde{\gamma}I_2 - \tilde{\nu}I_2 - dI_2,\\
\frac{dR_2}{dt} &= \gamma I_2 - \tilde{\xi}R_2 - dR_2,\\
\frac{\partial B_2}{\partial t} + \mathbf{v}_2\cdot\nabla B_2 &= D_2\nabla^2 B_2 + \tilde{\alpha}I_2 + q_{12}(t)B_1 - z_2B_2,\\
\frac{dS_3}{dt} &= \mu + \tilde{\xi}R_3 - \tilde{\beta}\frac{I_3}{N_3}S_3 - \tilde{\eta}\frac{B_3}{K+B_3}S_3 - dS_3,\\
\frac{dE_3}{dt} &= \tilde{\beta}\frac{I_3}{N_3}S_3 + \tilde{\eta}\frac{B_3}{K+B_3}S_3 - \tilde{\sigma}E_3 - dE_3 + m_{13}I_1(t) + m_{23}I_2(t).\\
\frac{dI_3}{dt} &= \tilde{\sigma}E_3 - \tilde{\gamma}I_3 - \tilde{\nu}I_3 - dI_3,\\
\frac{dR_3}{dt} &= \tilde{\gamma}I_3 - \tilde{\xi}R_3 - dR_3,\\
\frac{\partial B_3}{\partial t} + \mathbf{v}_3\cdot\nabla B_3 &= D_3\nabla^2 B_3 + \tilde{\alpha}I_3 - z_3B_3.
\end{aligned}
\tag{2.3}
$$

3 Epidemiological Analysis

3.1 Existence, Uniqueness, & Positivity of Solutions

Theorem 3.1 (Well-posedness of the Bacterial Transport Subsystem)**.** *Let $\Omega \subset \mathbb{R}^n$ be a bounded domain with smooth boundary and $T > 0$. The bacterial transport system* (2.2)*, subject to nonnegative initial data $B_i(0,x) \geq 0$ and homogeneous Neumann boundary conditions, admits*

a unique weak solution on $[0,T]$ *satisfying*

$$B_i \in C([0,T]; L^2(\Omega)) \cap L^2(0,T; H^1(\Omega)).$$

Moreover, solutions remain nonnegative for all $t \in [0,T]$*. The full proof is given in Appendix A.*

Theorem 3.2 (Well-posedness of the Human SEIR Subsystem)**.** *For each Region* $i \in \{1,2,3\}$*, the human SEIR system* (2.1) *admits a unique global solution for all* $t \geq 0$ *whenever the initial conditions satisfy*

$$S_i(0),\ E_i(0),\ I_i(0),\ R_i(0) \geq 0 \quad \textit{with} \quad N_i(0) > 0.$$

Moreover, solutions remain nonnegative for all time, and the total population $N_i(t)$ *remains bounded on finite time intervals. Consequently, the human SEIR subsystem is well posed. The full proof is provided in Appendix B.*

3.2 Global Asymptotic Stability of the DFE, $\Lambda_i = \Pi_i = 0$

Theorem 3.3 (Local Stability of the Disease-Free Equilibrium)**.** *Consider the cholera transmission model defined by System* (2.3)*, which admits a disease-free equilibrium (DFE)* $\mathcal{E}_0$*. Let* $\mathcal{R}_0$ *denote the basic reproduction number, defined as the spectral radius of the associated next-generation matrix. Then* $\mathcal{E}_0$ *is locally asymptotically stable if* $\mathcal{R}_0 < 1$ *and unstable if* $\mathcal{R}_0 > 1$*.*

Proof. The Disease-Free Equilibrium (DFE) of System 2.3 is

$$\begin{aligned}\mathcal{E}_0 &= \left(N_1^*, E_1^*, I_1^*, R_1^*, B_1^*, N_2^*, E_2^*, I_2^*, R_2^*, B_2^*, N_3^*, E_3^*, I_3^*, R_3^*, B_3^*\right) \\ &= \left(\frac{\mu}{d}, 0, 0, 0, 0, \frac{\mu}{d}, 0, 0, 0, 0, \frac{\mu}{d}, 0, 0, 0, 0\right)\end{aligned}$$

To assess the local stability of the DFE, we apply the next-generation matrix method of van den Driessche and Watmough (van den Driessche and Watmough, 2002). We define the infected state vector as $\mathbf{x} = \begin{bmatrix} E_i \\ I_i \\ B_i \end{bmatrix}$. Recall, $N_i = S_i + E_i + I_i + R_i$. We define the Jacobian Matrix, $\mathcal{J}$, with respect to $\mathbf{x}$ and evaluate it at the DFE:

$$J(\mathcal{E}_0) = \begin{bmatrix} -\sigma - d & \beta & \frac{\eta\mu}{Kd} & 0 & 0 & 0 & 0 & 0 & 0 \\ \sigma & -d-\gamma-\nu & 0 & 0 & 0 & 0 & 0 & 0 & 0 \\ 0 & \alpha & -q_{12} - z_1 & 0 & 0 & 0 & 0 & 0 & 0 \\ 0 & 0 & 0 & -\sigma - d & \beta & \frac{\eta\mu}{Kd} & 0 & 0 & 0 \\ 0 & 0 & 0 & \sigma & -d-\gamma-\nu & 0 & 0 & 0 & 0 \\ 0 & 0 & q_{12} & 0 & \alpha & -z_2 & 0 & 0 & 0 \\ 0 & m_{13} & 0 & 0 & m_{23} & 0 & -\sigma - d & \beta & \frac{\eta\mu}{Kd} \\ 0 & 0 & 0 & 0 & 0 & 0 & \sigma & -d-\gamma-\nu & 0 \\ 0 & 0 & 0 & 0 & 0 & 0 & 0 & \alpha & -z_3 \end{bmatrix}$$

Let $\mathcal{F}(\mathbf{x})$ denote the vector of new infection terms, and $\mathcal{V}(\mathbf{x})$ represent the vector of transitions between infected compartments. At the DFE, we compute the Jacobian matrix, $\mathcal{J}$ with respect to $\mathbf{x}$ and .

$$\mathcal{J}(\mathcal{E}_0) = \mathcal{F} - \mathcal{V}$$

where:

$$\mathcal{F} = \begin{bmatrix} 0 & \beta & \frac{\eta\mu}{Kd} & 0 & 0 & 0 & 0 & 0 & 0 \\ 0 & 0 & 0 & 0 & 0 & 0 & 0 & 0 & 0 \\ 0 & 0 & 0 & 0 & 0 & 0 & 0 & 0 & 0 \\ 0 & 0 & 0 & 0 & \beta & \frac{\eta\mu}{Kd} & 0 & 0 & 0 \\ 0 & 0 & 0 & 0 & 0 & 0 & 0 & 0 & 0 \\ 0 & 0 & 0 & 0 & 0 & 0 & 0 & 0 & 0 \\ 0 & 0 & 0 & 0 & 0 & 0 & 0 & \beta & \frac{\eta\mu}{Kd} \\ 0 & 0 & 0 & 0 & 0 & 0 & 0 & 0 & 0 \\ 0 & 0 & 0 & 0 & 0 & 0 & 0 & 0 & 0 \end{bmatrix}$$

$$\mathcal{V} = \begin{bmatrix} \sigma+d & 0 & 0 & 0 & 0 & 0 & 0 & 0 & 0 \\ -\sigma & d+\gamma+\nu & 0 & 0 & 0 & 0 & 0 & 0 & 0 \\ 0 & -\alpha & q_{12}+z_1 & 0 & 0 & 0 & 0 & 0 & 0 \\ 0 & 0 & 0 & \sigma+d & 0 & 0 & 0 & 0 & 0 \\ 0 & 0 & 0 & -\sigma & d+\gamma+\nu & 0 & 0 & 0 & 0 \\ 0 & 0 & -q_{12} & 0 & -\alpha & z_2 & 0 & 0 & 0 \\ 0 & -m_{13} & 0 & 0 & -m_{23} & 0 & \sigma+d & 0 & 0 \\ 0 & 0 & 0 & 0 & 0 & 0 & -\sigma & d+\gamma+\nu & 0 \\ 0 & 0 & 0 & 0 & 0 & 0 & 0 & -\alpha & z_3 \end{bmatrix}$$

The Basic Reproduction Number, $\mathcal{R}_0$, is defined as the spectral radius, maximum eigenvalue, of the matrix FV^{-1}:

$$\begin{aligned}
\mathcal{R}_0 &= \max\left\{ \frac{\tilde{\sigma}\left(\tilde{\beta}Kdz_3+\tilde{\eta}\mu\alpha\right)}{Kd\left(d+\gamma+\tilde{\nu}\right)\left(\tilde{\sigma}+d\right)z_3}, \frac{\tilde{\sigma}\left(K\tilde{\beta}dz_2+\tilde{\eta}\mu\tilde{\alpha}\right)}{Kd\left(d+\tilde{\gamma}+\tilde{\nu}\right)\left(\tilde{\sigma}+d\right)z_2}, \frac{\tilde{\sigma}\left(K\beta dq_{12}+K\tilde{\beta}dz_1+\tilde{\eta}\mu\tilde{\alpha}\right)}{Kd\left(d+\tilde{\gamma}+\tilde{\nu}\right)\left(\tilde{\sigma}+d\right)\left(q_{12}+z_1\right)} \right\} \\
&= \max\Big\{ \frac{\tilde{\beta}\tilde{\sigma}}{\left(\tilde{\sigma}+d\right)\left(d+\tilde{\gamma}+\tilde{\nu}\right)} + \frac{\tilde{\eta}\mu\tilde{\alpha}\tilde{\sigma}}{Kd\left(d+\tilde{\gamma}+\tilde{\nu}\right)\left(\tilde{\sigma}+d\right)z_3}, \\
&\qquad \frac{\tilde{\beta}\tilde{\sigma}}{\left(\tilde{\sigma}+d\right)\left(d+\tilde{\gamma}+\tilde{\nu}\right)} + \frac{\tilde{\eta}\mu\tilde{\alpha}\tilde{\sigma}}{Kd\left(d+\gamma+\nu\right)\left(\tilde{\sigma}+d\right)z_2}, \\
&\qquad \frac{\tilde{\beta}\tilde{\sigma}}{\left(\tilde{\sigma}+d\right)\left(d+\tilde{\gamma}+\tilde{\nu}\right)} + \frac{\tilde{\eta}\mu\alpha\sigma}{Kd\left(d+\gamma+\nu\right)\left(\sigma+d\right)\left(q_{12}+z_1\right)} \Big\} \\
&= \frac{\tilde{\beta}\tilde{\sigma}}{\left(\tilde{\sigma}+d\right)\left(d+\tilde{\gamma}+\tilde{\nu}\right)} + max\left\{ \frac{\eta\mu\tilde{\alpha}\sigma}{Kd\left(d+\tilde{\gamma}+\tilde{\nu}\right)\left(\tilde{\sigma}+d\right)z_3}, \frac{\eta\mu\alpha\sigma}{Kd\left(d+\tilde{\gamma}+\tilde{\nu}\right)\left(\tilde{\sigma}+d\right)z_2}, \frac{\tilde{\eta}\mu\tilde{\alpha}\tilde{\sigma}}{Kd\left(d+\tilde{\gamma}+\tilde{\nu}\right)\left(\tilde{\sigma}+d\right)\left(q_{12}+z_1\right)} \right\} \\
&= \frac{\beta\sigma}{(\sigma+d)(d+\gamma+\nu)} + \frac{\eta\mu\tilde{\alpha}\tilde{\sigma}}{Kd(d+\tilde{\gamma}+\tilde{\nu})(\tilde{\sigma}+d)} \max\left\{ \frac{1}{z_3}, \frac{1}{z_2}, \frac{1}{q_{12}+z_1} \right\} \\
&=: R_H + R_B \cdot \Psi_B.
\end{aligned}$$

where,

$$R_H := \frac{\tilde{\beta}\tilde{\sigma}}{(\tilde{\sigma}+d)(d+\tilde{\gamma}+\tilde{\nu})}, \quad R_B := \frac{\tilde{\eta}\mu\tilde{\alpha}\tilde{\sigma}}{Kd(d+\tilde{\gamma}+\tilde{\nu})(\tilde{\sigma}+d)}, \quad \Psi_B := \max\left\{ \frac{1}{z_3}, \frac{1}{z_2}, \frac{1}{q_{12}+z_1} \right\}$$

A result of the Next Generation Method assures us that if $\mathcal{R}_0 < 1$, the DFE is Locally Asymptotically Stable. Conversely, if $\mathcal{R}_0 > 1$, the DFE is unstable. □

The basic reproduction number decomposes as $\mathcal{R}_0 = R_H + R_B\,\Psi_B$, separating direct human transmission from environmentally mediated transmission. The term R_H captures person-to-person spread, while $R_B\,\Psi_B$ represents environmental amplification governed by the dominant bacterial persistence pathway, reflecting a bottleneck determined by the slowest effective removal or flushing process.

This structure shows that cholera persistence arises from the interaction of human transmission and environmental amplification shaped by hydrological transport and spatial heterogeneity. Effective control therefore requires simultaneous reduction of direct transmission and environmental persistence, particularly in regions with slow bacterial clearance.

Notably, $\mathcal{R}_0$ is independent of the external importation term $\Pi_i(t)$, reflecting a limitation of threshold

quantities derived from linearization about the disease-free equilibrium. While $\mathcal{R}_0 < 1$ guarantees elimination in the absence of external inputs, sustained importation ($\Pi_i(t) \neq 0$) can maintain transmission under subcritical local dynamics. In the Haitian context, $\Pi_i(t)$ may represent infection pressure from population movement or external intervention, indicating reducing $\mathcal{R}_0$ below unity is necessary but not sufficient for eradication.

3.3 Global Asymptotic Stability of the DFE $(\Lambda_i = \Pi_i = 0)$

Theorem 3.4 (Global Asymptotic Stability of the DFE)**.** *Consider the three-region SEIR-B cholera model* (2.3)*. Assume there is no exogenous environmental contamination or external infection importation, i.e.,*

$$\Lambda_i(t) \equiv 0 \quad \textit{and} \quad \Pi_i(t) \equiv 0, \qquad i = 1, 2, 3.$$

Define the Lyapunov function

$$\mathcal{L}(t) = a \sum_{i=1}^{3} E_i^2 + b \sum_{i=1}^{3} I_i^2 + \sum_{i=1}^{3} c_i B_i^2,$$

with constants $a, b, c_i > 0$ chosen appropriately. If the basic reproduction number satisfies $\mathcal{R}_0 < 1$, then

$$\dot{\mathcal{L}}(t) \leq 0,$$

with equality only at the DFE $\mathcal{E}_0$. Consequently, $\mathcal{E}_0$ is globally asymptotically stable. The proof is given in Appendix C.

3.4 Final Epidemic Size Relation

The *final size relation* links the susceptible population at the beginning and end of an epidemic, providing an implicit measure of cumulative outbreak burden without resolving full transient dynamics. If u_i denotes the proportion of individuals in Region i remaining susceptible at epidemic termination, then $1 - u_i$ represents the total fraction infected. In models with both direct and environmentally mediated transmission, the final size relation decomposes into human and environmental components, yielding a transcendental equation for u_i that depends on key epidemiological parameters, including $\mathcal{R}_0$.

Theorem 3.5 (Final Epidemic Size Relation)**.** *Let*

$$u_i := \frac{S_i(T)}{S_i(0)} \in (0, 1)$$

denote the proportion of individuals in Region i remaining susceptible at the end of a single epidemic wave over $[0, T]$. Under the epidemic time-scale approximation, the final size relation satisfies

$$\ln\left(\frac{1}{u_i}\right) = \mathcal{R}_0 \left(1 - u_i\right) + \mathcal{E}_i,$$

where $\mathcal{R}_0$ is the basic reproduction number associated with endogenous transmission and

$$\mathcal{E}_i := \tilde{\lambda} \int_0^T \frac{B_i(t)}{K + B_i(t)}\, dt$$

is the cumulative environmental infection pressure in Region i. In the absence of environmental exposure ($\mathcal{E}_i = 0$), this reduces to the classical final size equation $\ln(1/u_i) = \mathcal{R}_0(1 - u_i)$. The derivation is given in Appendix D.

Corollary 3.6 (Threshold Behavior of the Basic Reproduction Number)**.** *Suppose the final size relation*

$$\ln\left(\frac{1}{u_i}\right) = \mathcal{R}_0(1 - u_i) + \mathcal{E}_i, \qquad \mathcal{E}_i \geq 0,$$

holds. Then:

- *If $\mathcal{R}_0 < 1$ and $\mathcal{E}_i = 0$, the only solution is $u_i \to 1$, yielding a negligible final epidemic size.*
- *If $\mathcal{R}_0 > 1$, there exists a solution $u_i < 1$, corresponding to a nontrivial outbreak.*
- *If $\mathcal{R}_0 < 1$ but $\mathcal{E}_i > 0$, environmental exposure can still induce a positive final epidemic size despite subcritical endogenous transmission.*

Thus, $\mathcal{R}_0 = 1$ remains the threshold for invasion driven by local transmission, while environmental forcing modifies outbreak magnitude without altering the intrinsic threshold.

This approximation is most accurate for large populations and single-wave epidemics, where stochastic effects, demographic turnover, reinfection, and spatial heterogeneity are negligible. Despite these limitations, the final size relation provides useful analytical insight for short- to moderate-duration outbreaks in homogeneous settings. In contrast to prior work on COVID-19 dynamics (Thomas, 2024), where the final size relation was obtained as an inequality using age-of-infection models and bounding arguments, the present study employs a deterministic compartmental framework and derives an exact equality by direct integration of the susceptible equation.

3.5 Thresholds for Bacterial Persistence and Elimination

Theorem 3.7 (Global Stability of the Bacteria-Free State)**.** *Consider the bacterial concentration $B_i(t, x)$ in Region $i \in \{1, 2, 3\}$ governed by*

$$\frac{\partial B_i}{\partial t} + \mathbf{v}_i \cdot \nabla B_i = D_i \nabla^2 B_i + \tilde{\alpha}\, I_i + \sum_{j \neq i} q_{ji}(t)\, B_j - \sum_{j \neq i} q_{ij}(t)\, B_i - z_i B_i + \Lambda_i(t),$$

with nonnegative initial data $B_i(0, x) \geq 0$. Define the bacterial persistence threshold

$$\mathcal{Q}_B := \max_{i \in \{1,2,3\}} \frac{\tilde{\alpha}\, I_{\max} + \Lambda_{\max}}{z_i + \sum_{j \neq i} \underline{q}_{ij}},$$

where $I_{\max}$ and $\Lambda_{\max}$ are uniform upper bounds on $I_i(t, x)$ and $\Lambda_i(t)$, and $\underline{q}_{ij}$ is a positive lower bound on $q_{ij}(t)$. If $\mathcal{Q}_B < 1$, then the bacteria-free equilibrium

$$B_i^*(x) \equiv 0, \qquad i \in \{1, 2, 3\},$$

is globally asymptotically stable, i.e., $B_i(t, x) \to 0$ as $t \to \infty$ for all admissible initial conditions. The proof is given in Appendix E.

The threshold $\mathcal{Q}_B$ quantifies the balance between bacterial input and effective removal. The numerator represents bacterial introduction through human shedding and exogenous environmental contamination, while the denominator captures removal via natural decay, sanitation, and hydrological export. When $\mathcal{Q}_B < 1$, bacterial concentrations decay to zero for all admissible initial conditions; when $\mathcal{Q}_B > 1$, environmental contamination persists and can sustain transmission.

From a control perspective, elimination can be achieved by reducing shedding, enhancing bacterial clearance, increasing hydrological flushing, or limiting external inputs. Accordingly, $\mathcal{Q}_B$ provides a practical criterion for determining whether local interventions suffice or coordinated multi-region control is required.

3.6 Intervention Effects and Structural Risk

We analyze the effects of interventions on environmental bacterial persistence using analytical tools including Lyapunov stability, monotonicity arguments, and threshold analysis. This framework identifies conditions under which interventions successfully eliminate environmental reservoirs, as well as regimes in which well-intended external actions may inadvertently sustain bacterial persistence by introducing persistent environmental forcing.

Theorem 3.8 (Monotone Effect of Exogenous Contamination on Environmental Persistence)**.** *Consider the bacterial concentration in Region i governed by*

$$\frac{\partial B_i}{\partial t} + \mathbf{v}_i \cdot \nabla B_i = D_i \nabla^2 B_i + \tilde{\alpha}\, I_i + \sum_{j \neq i} q_{ji}(t)\, B_j - \sum_{j \neq i} q_{ij}(t)\, B_i - z_i B_i + \Lambda_i(t),$$

where all parameters are nonnegative, $z_i > 0$, and $\Lambda_i(t) \geq 0$ represents exogenous environmental contamination. Assume spatial homogeneity (or spatial averaging with zero-flux boundary conditions), bounded transport rates $q_{ij}(t)$, and uniformly bounded $I_i(t)$. Then the reduced mean bacterial dynamics admit a unique nonnegative equilibrium B_i^*, which depends strictly monotonically *on Λ_i. In particular,*

$$\frac{\partial B_i^*}{\partial \Lambda_i} > 0 \qquad \textit{whenever } B_i^* > 0.$$

Moreover, if $I_i \equiv 0$ and $\Lambda_i > 0$, the system admits a unique positive environmental equilibrium, whereas if $I_i \equiv 0$ and $\Lambda_i \equiv 0$, the bacteria-free state $B_i^* = 0$ is globally asymptotically stable. The proof is given in Appendix F.

Theorem 3.8 establishes that any persistent external input $\Lambda_i > 0$ sustains a nonzero environmental bacterial reservoir, even in the absence of local human infection. Exogenous contamination therefore acts as a *structural forcing mechanism*, elevating long-term environmental burden independently of endogenous transmission dynamics.

In the Haitian context, the 2010 introduction of cholera by UN peacekeepers (Katz, 2016; Frerichs, 2016; Orata et al., 2014) may be interpreted as a sustained increase in Λ_i due to contaminated waste discharge into the Artibonite River system. Under transport-driven dynamics, such forcing necessarily shifts the system to a higher environmental equilibrium, facilitating persistence and downstream spread. This provides a mathematical formalization of observations documented in epidemiological, historical, and sociological studies: well-intended external interventions can introduce structural risks

that persist beyond the initiating event. Within this framework, the Western savior complex is not modeled as intent, but as a *mechanism of exogenous environmental forcing*, whereby externally imposed actions alter system dynamics in ways local control measures alone cannot reverse (Farmer, 2011; Dubois, 2012; Jean-Louis, 2020).

4 Numerical Simulations

4.1 Parameter Values and Simulation Setup

We specify the baseline parameter values, initial conditions, and numerical methods used in all simulations, including the simulation horizon, integration scheme, spatial structure, and implementation of aquatic transport $q_{ij}(t)$ and exogenous environmental contamination $\Lambda_i(t)$.

All simulations use the baseline parameter values listed in Tables 2-3, which define demographic dynamics, disease progression, environmental transmission, bacterial decay, and hydrological coupling across the three regions. Initial conditions were chosen to reflect heterogeneous regional disease burden and environmental exposure. Unless stated otherwise, simulations were conducted over a one-year horizon $t \in [0, 365]$ using the stiff solver `ode15s` with relative tolerance 10^{-7} and absolute tolerance 10^{-9}.

Hydrological transport was modeled through a constant downstream coupling rate q_{12} from Region (1) to Region (2), while Region (3) was treated as environmentally isolated. Exogenous contamination was introduced via a constant forcing term Λ_1 applied to the upstream region. Sensitivity to external contamination was examined by varying Λ_1 while holding all other parameters fixed.

Table 2: Baseline parameter values used in numerical simulations. City indices correspond to (1) Mirebalais, (2) Gonaïves, and (3) Port-au-Prince.

Parameter	Value	Source
μ	$1/(65 \times 365)$	(Codeço, 2001; World Health Organization, 2023)
d	$1/(70 \times 365)$	(World Health Organization, 2023) (United Nations, 2022)
β	0.04-0.08	(Tuite et al., 2011; Eisenberg et al., 2013)
η	0.2-0.4	(Mukandavire et al., 2011)
σ	$1/5$	(Centers for Disease Control and Prevention, 2023)
γ	$1/7$	(Centers for Disease Control and Prevention, 2023; Codeço, 2001)
ν	0.001-0.005	(World Health Organization, 2011–2019; Pan American Health Organization, 2019)
ξ	$1/(3\text{-}5 \times 365)$	(Koelle et al., 2005).
α	0.05-0.2	(Hartley et al., 2006).
K	10^4	(Codeço, 2001).
z_1	0.3-0.5	(Hartley et al., 2006).

Continued on next page

Parameter	Value	Source
z_2	0.3-0.5	(Mukandavire et al., 2011)
z_3	0.3	(Eisenberg et al., 2013)
q_{12}	0.1	(Tuite et al., 2011)
m_{13}	0.005	(International Organization for Migration, 2011; Tuite et al., 2011)
m_{23}	0.002	(International Organization for Migration, 2011)

Table 3: Initial conditions for epidemiological compartments and bacterial concentrations used in numerical simulations. City indices correspond to (1) Mirebalais, (2) Gonaïves, and (3) Port-au-Prince.

Region	$S_i(0)$	$E_i(0)$	$I_i(0)$	$R_i(0)$	$B_i(0)$	Justification / Source
Mirebalais (1)	5.0×10^2	8	2	0	10^{-6}	(Piarroux et al., 2011; Tuite et al., 2011)
Gonaïves (2)	8.0×10^2	10	5	0	10^{-6}	(Barzilay et al., 2013; Tuite et al., 2011)
Port-au-Prince (3)	9.0×10^2	15	10	0	10^{-6}	(Piarroux et al., 2011; Tuite et al., 2011; Ivers and Walton, 2013)

We vary the exogenous contamination input $\Lambda_1(t)$ over magnitudes scaled to endogenous shedding,

$$\Lambda_1(t) = L\,\mathbb{I}_{[t_0,t_1]}(t), \qquad L \in \{0, 0.1, 0.25, 0.5, 1, 2, 5\} \times (\alpha I_{\mathrm{ref}}),$$

so external forcing ranges from negligible to several-fold larger than the typical internal contribution $\tilde{\alpha}I$. Initial conditions reflect relative outbreak timing and hydrological connectivity rather than exact case counts, and results are robust to moderate variation in these values.

4.2 Numerical Results in a Three-Region Hydrological Network

Figures 2 and 3 show the baseline dynamics of the three-region SEIR-B system with no exogenous environmental contamination($\Lambda_i(t) \equiv 0$). Figure 2 displays the infectious populations $I_1(t)$, $I_2(t)$, and $I_3(t)$, while Figure 3 shows the corresponding bacterial concentrations $B_1(t)$, $B_2(t)$, and $B_3(t)$.
Under baseline conditions, transmission arises solely from endogenous processes, including direct human-to-human spread and locally generated environmental reservoirs. The infection trajectories in Figure 2 exhibit distinct regional epidemic patterns driven by heterogeneous initial conditions and asymmetric network coupling. Although Region (3) receives no environmental input via hydrological transport, its infection dynamics are indirectly influenced by upstream regions through human migration.

The bacterial dynamics in Figure 3 reflect the underlying hydrological network: Region (1) acts as an upstream bacterial source, Region (2) receives downstream inflow, and Region (3) remains environmentally isolated, with bacterial concentrations governed solely by local shedding and natural decay.

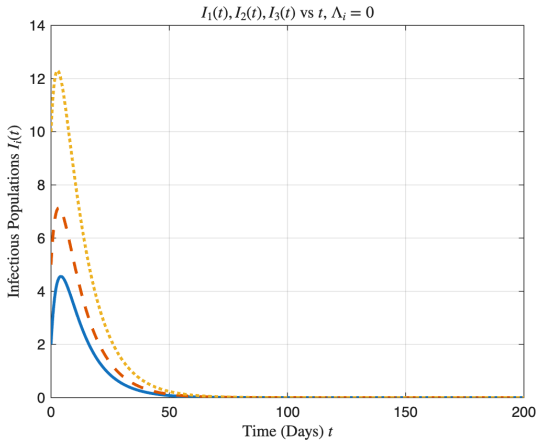

Figure 2: Temporal evolution of the infectious populations $I_1(t)$, $I_2(t)$, and $I_3(t)$ in the three-region SEIR-B model under baseline conditions with no exogenous environmental contamination ($\Lambda_i(t) \equiv 0$).

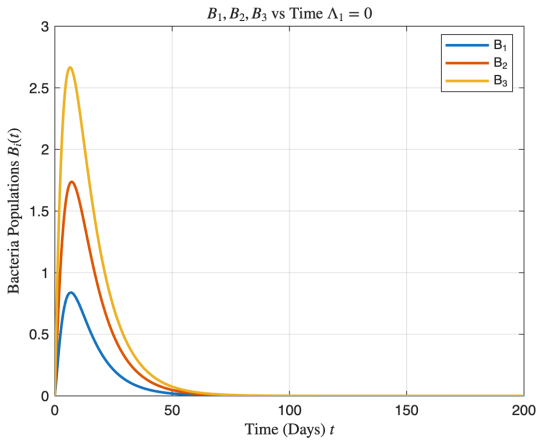

Figure 3: Time evolution of environmental bacterial concentrations $B_1(t)$, $B_2(t)$, and $B_3(t)$ under baseline conditions with $\Lambda_i(t) \equiv 0$.

Together, these simulations characterize the intrinsic coupling between infection and environmental contamination in the absence of external forcing, providing a baseline for assessing the effects of exogenous contamination, control interventions, and transport intensity in subsequent sections.

Figures 4-6 illustrate the effects of time-dependent exogenous environmental contamination on bacterial dynamics in the three-region hydrological network. An external input $\Lambda_1(t)$ is applied to the upstream region while all other parameters remain at baseline values, isolating the impact of exogenous contamination from endogenous transmission.

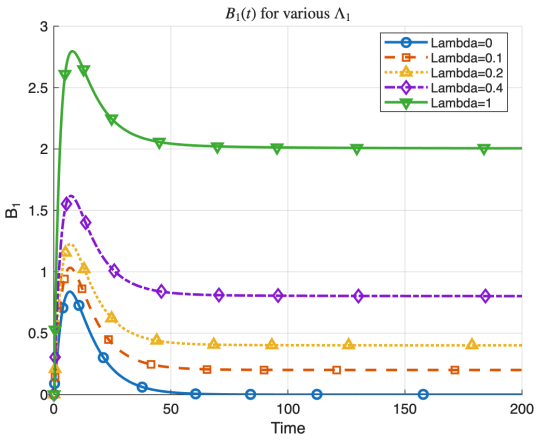

Figure 4: Environmental bacterial concentration $B_1(t)$ in the upstream region for increasing magnitudes of the exogenous contamination input $\Lambda_1(t)$.

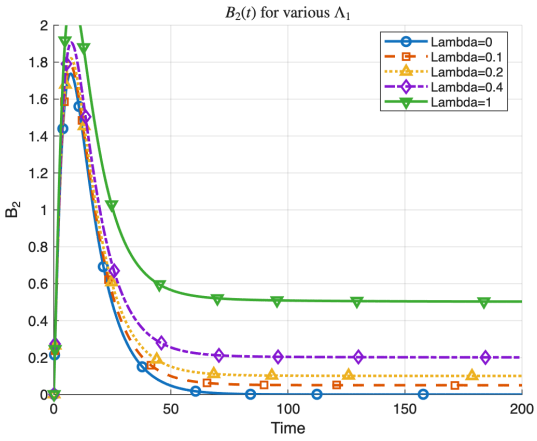

Figure 5: Environmental bacterial concentration $B_2(t)$ in the downstream region under increasing upstream contamination $\Lambda_1(t)$.

As shown in Figure 4, increasing the magnitude of $\Lambda_1(t)$ produces a monotone increase in the bacterial concentration $B_1(t)$ in the upstream region. Elevated bacterial levels propagate downstream

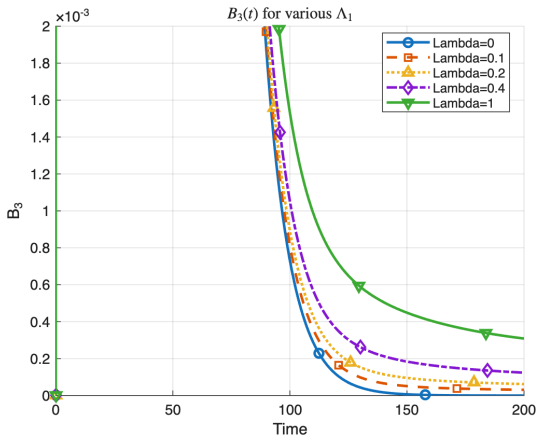

Figure 6: Environmental bacterial concentration $B_3(t)$ in the environmentally isolated region.

to Region (2) via aquatic transport (Figure 5), while Region (3) shows no direct bacterial response, reflecting its environmental isolation (Figure 6). The corresponding infection dynamics (Figures 7-9) exhibit only modest sensitivity to $\Lambda_1(t)$, as exogenous contamination influences prevalence indirectly through environmental and migratory coupling, particularly in regions without direct environmental inflow.

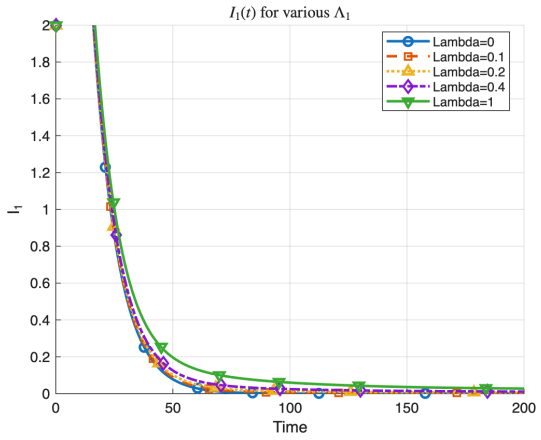

Figure 7: Infectious population $I_1(t)$ in the upstream region for varying magnitudes of $\Lambda_1(t)$.

These numerical results are consistent with the analytical monotonicity result in Theorem 3.8, which predicts sustained external contamination prevents bacterial elimination in affected regions. Together, the simulations confirm exogenous inputs act as a dominant driver of environmental persistence, while downstream epidemiological effects depend critically on network structure and coupling pathways. The analytical results identify conditions under which environmental reservoirs of *Vibrio cholerae* can be eliminated through reductions in bacterial shedding and environmental

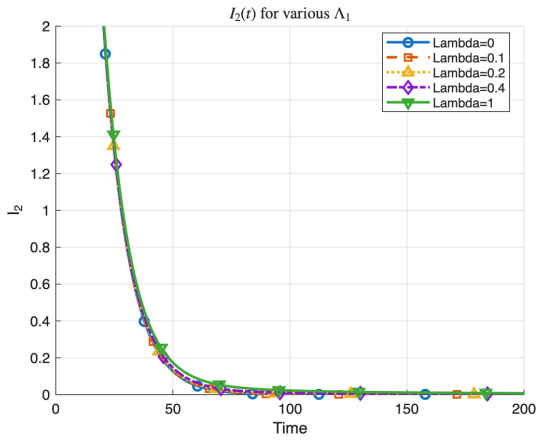

Figure 8: Infectious population $I_2(t)$ in the downstream region under increasing upstream contamination.

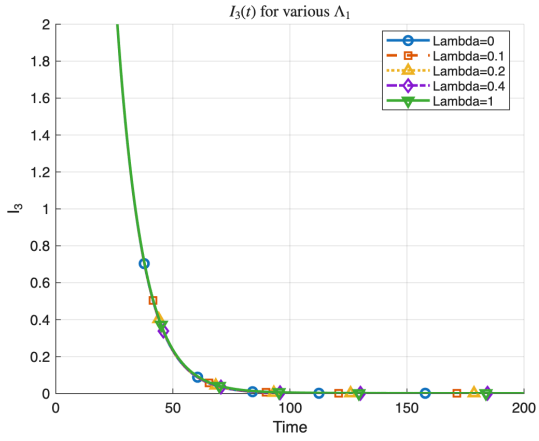

Figure 9: Infectious population $I_3(t)$ in the environmentally isolated region.

transmission, revealing a threshold separating persistence from elimination. Although the numerical simulations do not explicitly vary sanitation or shedding parameters, the strong sensitivity of bacterial dynamics to environmental inputs highlights the central role of these mechanisms in sustaining infection. In the absence of sufficient control, bacterial reservoirs persist at positive endemic levels, whereas sufficiently strong reductions in shedding or environmental transmission are predicted to suppress persistence and drive elimination. Taken together, the theoretical and numerical results underscore environmental control measures, such as improved sanitation and reduced pathogen shedding, are essential components of effective intervention strategies, even in the absence of ongoing exogenous contamination.

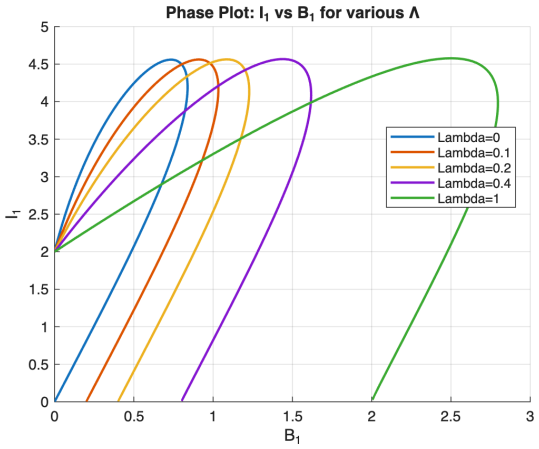

Figure 10: Phase-plane trajectories of $I_1(t)$ versus $B_1(t)$ in the upstream region under varying $\Lambda_1(t)$.

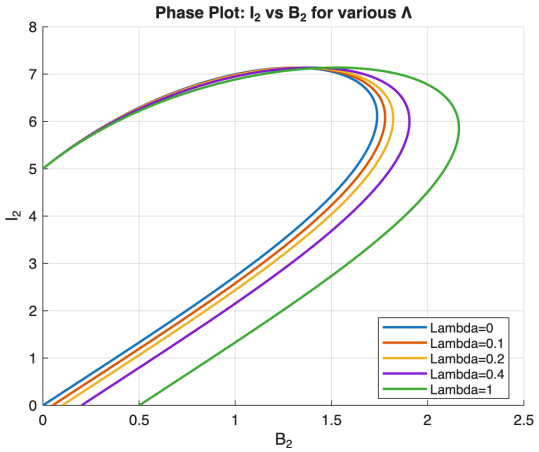

Figure 11: Phase-plane trajectories of $I_2(t)$ versus $B_2(t)$ in the downstream region.

Although the analytical results identify conditions for eliminating environmental reservoirs through sanitation and shedding control, the numerical simulations here focus on exogenous contamination and aquatic coupling. Accordingly, explicit variation of sanitation or shedding parameters is not

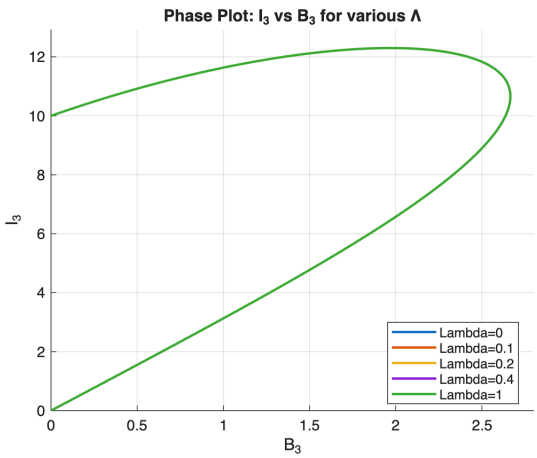

Figure 12: Phase-plane trajectories of $I_3(t)$ versus $B_3(t)$ in the environmentally isolated region.

shown. Nonetheless, the simulations demonstrate bacterial persistence is strongly governed by environmental feedback, suggesting that reductions in shedding and environmental transmission would be decisive for elimination. A systematic numerical study of sanitation-driven thresholds is deferred to future work.

5 Discussion

5.1 Interpretation of Numerical Results

We examine cholera dynamics in a three-region system where transmission occurs through both direct contact and environmental exposure, and environmental bacteria evolve via shedding, decay, and hydrological transport. The upstream region includes both an outflow term $-q_{12}(t)B_1$ and an external forcing term $\Lambda_1(t)$, while the downstream region receives bacterial inflow through $q_{12}(t)B_1$. This structure distinguishes persistence driven by endogenous transmission from persistence maintained by sustained exogenous contamination.

Baseline simulations (Figures 2-3) show when exogenous contamination is absent $(\Lambda_i \equiv 0)$, bacteria arise solely from infection-driven shedding and are attenuated by decay and hydrological loss. Under these conditions, large transient outbreaks may still occur, accompanied by a rise-and-fall response in environmental reservoirs (Figure 3), demonstrating the amplifying role of environmental feedback even in the absence of external forcing.

Forcing experiments show upstream environmental inputs propagate downstream through aquatic coupling. Increasing $\Lambda_1(t)$ elevates the upstream reservoir $B_1(t)$ (Figure 4), which in turn increases the downstream reservoir $B_2(t)$ via the transport term $q_{12}(t)B_1$ (Figure 5). Correspondingly, infection trajectories exhibit increased outbreak magnitude and persistence as $\Lambda_1(t)$ increases (Figures 7-9), indicating local disease control can be undermined by persistent upstream contamination.

In contrast, Region 3 is environmentally isolated and receives neither water inflow nor direct forcing. As a result, its bacterial reservoir $B_3(t)$ is governed primarily by local shedding and decay and

exhibits weak sensitivity to changes in Λ_1 (Figures 6, 12). More generally, these results highlight in environmentally uncoupled regions, upstream contamination affects local dynamics primarily through human mobility rather than waterborne pathways.

5.2 Limitations and Next Numerical steps

The present simulations were designed to isolate the role of upstream forcing and a single hydrological connection. Several natural extensions would strengthen the quantitative interpretation:

- **Systematic sensitivity to sanitation and shedding control.** Varying environmental transmission (e.g., $\tilde{\eta}$) and shedding (e.g., $\tilde{\alpha}$) would directly test the predicted persistence/elimination threshold behavior under environmental control.
- **General hydrological networks.** Extending the transport structure beyond a single edge (e.g., adding $q_{23}(t)$ or multi-edge routing) would clarify when upstream forcing can affect otherwise weakly connected regions.
- **Time-varying and pulsed forcing.** Replacing constant Λ_1 levels with episodic or seasonal inputs would better reflect rainfall-driven contamination and infrastructural shocks.
- **Homogeneous Mixing Within Regions.** The model assumes uniform mixing of individuals within each region, neglecting spatial heterogeneity such as urban vs. rural settings, slums vs. affluent areas, or localized outbreaks within a region.
- **No Age or Demographic Structure.** Individuals are treated as demographically identical. Age-related differences in susceptibility, mortality, mobility, and vaccination status are not included, despite evidence that children and the elderly may be more vulnerable to cholera.
- **Vaccination Modeled as Static Reduction Coefficients.** Vaccine efficacy is modeled through constant reduction parameters ($\epsilon_S, \epsilon_B, \epsilon_E, \epsilon_I, \epsilon_R$), assuming immediate and uniform effect. This does not account for waning immunity over time, multi-dose schedules, or individual-level heterogeneity in response.
- **No Explicit Migration of Human Compartments.** While bacterial movement is modeled via hydrological transport, the model does not explicitly incorporate human migration between regions. This omits the possibility of exposed or infectious individuals seeding outbreaks elsewhere.
- **Environmental Compartment is Spatially Continuous, but Human Compartments Are Not.** The bacterial concentration B_i evolves through advection and diffusion over space, but the human populations S_i, E_i, I_i, R_i are treated as regional aggregates without spatial diffusion or mobility across space.
- **Runoff-Based Bacterial Transfer Assumes Instantaneous Impact.** Inputs and outputs from other regions are applied instantly to the bacterial reservoir, not accounting for transport time delays or attenuation along hydrological routes.
- **Lack of Stochasticity.** The model is deterministic and does not incorporate random events such as rainfall variability, infrastructure failure, super-spreader events, or under-reporting noise that can drive cholera dynamics in real populations.
- **Simplified Environmental Decay and Removal.** The bacterial decay term z_i is linear and does not include thresholds, saturation effects, or nonlinearities that might arise in real water treatment systems or natural ecosystems.
- **No Feedback Between Human Behavior and Disease Prevalence.** The model does not include adaptive behavior such as increased sanitation during outbreaks, changes in water usage, or vaccine uptake as a function of perceived risk.
- **Assumes Accurate and Stable Infrastructure Parameters.** Infrastructure parameters such as water sanitation levels, are treated as constant and known, despite likely fluctuations in real-world implementation and quality of services.

- **No Explicit Climate or Weather Forcing.** Although rainfall-driven runoff is implicit in the bacterial transport parameters, the model does not dynamically include climate factors like seasonal rainfall, hurricanes, or temperature, which are known to influence cholera dynamics.
- **No Co-Infection or Interaction With Other Diseases.** The model isolates cholera without accounting for potential interactions with other gastrointestinal diseases, malnutrition, or parasitic infections that may alter susceptibility, severity, or transmission dynamics.
- **In-Transit Exposure Modeled Implicitly.** Exposure during transit is acknowledged in the narrative, but not represented through explicit compartments or transit-network structure in the differential equations.
- **Single Pathogen Strain Assumption.** The model assumes a single strain of Vibrio cholerae, ignoring the potential emergence or co-circulation of multiple serogroups or variants with different transmission, virulence, or immune response characteristics.
- **No Health System Constraints or Treatment Delays.** The model assumes access to recovery pathways ($\tilde{\gamma}$) without delays, shortages in oral rehydration, or overwhelmed healthcare systems that often accompany real outbreaks.

Conclusion:

Overall, the analytical framework and numerical experiments together support three main conclusions. First, environmental feedback can produce large transient outbreaks even in the absence of external inputs (Figures 2 - 3). Second, sustained upstream contamination $\Lambda_1(t)$ can maintain and amplify bacterial persistence in Region 1 and can elevate downstream bacterial burden through hydrological transport (Figures 4 - 5). Third, the sensitivity of each region depends sharply on the network structure: environmentally uncoupled regions may exhibit limited downstream response unless additional coupling mechanisms (e.g., hydrological links or stronger mobility terms) are present (Figures 6 and 12). These findings underscore the public-health implication that effective cholera mitigation in riverine systems requires coordinated regional strategies, that address both local transmission and upstream environmental sources.

References

M. Ali, A. R. Nelson, A. L. Lopez, and D. A. Sack. Updated global burden of cholera in endemic countries. *PLoS Neglected Tropical Diseases*, 14(6):e0008322, 2020. doi: 10.1371/journal.pntd.0008322.

H. Amann. *Linear and Quasilinear Parabolic Problems. Volume I: Abstract Linear Theory*, volume 89 of *Monographs in Mathematics*. Birkhäuser, Basel, 1995.

R. M. Anderson and R. M. May. *Infectious Diseases of Humans: Dynamics and Control*. Oxford University Press, 1991.

A. S. Azman, F. J. Luquero, I. Ciglenecki, R. F. Grais, D. A. Sack, and J. Lessler. The impact of cholera vaccination on cholera mortality and transmission. *The Lancet*, 387(10033):2462–2471, 2016. doi: 10.1016/S0140-6736(16)00501-8.

E. J. Barzilay, N. Schaad, R. Magloire, K. S. Mung, J. Boncy, G. Dahourou, and E. D. Mintz. Cholera surveillance during the haiti epidemic — the first two years. *The New England Journal of Medicine*, 368(7):599–609, 2013. doi: 10.1056/NEJMoa1204927.

E. Bertuzzo, L. Mari, L. Righetto, M. Gatto, R. Casagrandi, I. Rodriguez-Iturbe, and A. Rinaldo. Prediction of the spatial evolution and effects of control measures for the cholera outbreak in haiti. *PLoS Neglected Tropical Diseases*, 4(10):e899, 2010.

F. Brauer, C. Castillo-Chavez, and Z. Feng. *Mathematical Models in Epidemiology*. Springer, 2019.

L. Cai, Y. Kang, and J. Wu. An age-structured model for cholera control with vaccination. *Mathematical Biosciences*, 280:38–47, 2016.

Centers for Disease Control and Prevention. Cholera — general information, 2023. URL https://www.cdc.gov/cholera/general/index.html. Incubation period estimates.

Centers for Disease Control and Prevention. Isolation precautions guideline, 2024a. URL https://www.cdc.gov/infection-control/hcp/isolation-precautions/index.html.

Centers for Disease Control and Prevention. Legal authorities for isolation and quarantine, 2024b. URL https://www.cdc.gov/port-health/legal-authorities/isolation-quarantine.html.

C.-S. Chin, J. Sorenson, J. B. Harris, W. P. Robins, R. C. Charles, R. R. Jean-Charles, J. Bullard, and M. K. Waldor. The origin of the haitian cholera outbreak strain. *New England Journal of Medicine*, 364(1):33–42, Jan. 2011. doi: 10.1056/NEJMoa1012928.

C. T. Codeço. Endemic and epidemic dynamics of cholera: the role of the aquatic reservoir. *BMC Infectious Diseases*, 1(1):1, 2001. doi: 10.1186/1471-2334-1-1. URL https://doi.org/10.1186/1471-2334-1-1.

R. R. Colwell and et al. Reduction of cholera in bangladeshi villages by simple filtration. *Proceedings of the National Academy of Sciences*, 100(3):1051–1055, 2003.

O. Diekmann, J. A. P. Heesterbeek, and T. Britton. *Mathematical Tools for Understanding Infectious Disease Dynamics*. Princeton University Press, 2013.

L. Dubois. *Haiti: The Aftershocks of History*. Metropolitan Books, New York, 2012.

J. N. Eisenberg, M. A. Desai, K. Levy, S. J. Bates, S. Liang, K. Naumoff, and W. Cevallos. Environmental determinants of infectious disease: a framework for tracking causal links and guiding public health research. *Environmental Health Perspectives*, 115(8):1216–1223, 2013.

L. C. Evans. *Partial Differential Equations*, volume 19 of *Graduate Studies in Mathematics*. American Mathematical Society, 2nd edition, 2010.

P. Farmer. *Haiti After the Earthquake*. PublicAffairs, New York, 2011.

F. Finger, A. Knox, E. Bertuzzo, L. Mari, D. Bompangue, M. Gatto, A. Rinaldo, and A. S. Azman. Climate-driven cholera dynamics in haiti. *Proceedings of the National Academy of Sciences*, 113 (4):927–932, 2016. doi: 10.1073/pnas.1517452113.

R. R. Frerichs. *Deadly River: Cholera and Cover-Up in Post-Earthquake Haiti*. ILR Press, Ithaca, NY, 2016.

M. K. Gobbert and A. Agheksanterian. Modeling the spread of epidemic cholera: An age-structured model. Master's thesis, University of Maryland, Baltimore County, 2007.

D. M. Hartley, J. G. Morris Jr, and D. L. Smith. Hyperinfectivity: A critical element in the ability of v. cholerae to cause epidemics? *PLoS Medicine*, 3(1):e7, 2006.

H. W. Hethcote. The mathematics of infectious diseases. *SIAM Review*, 42(4):599–653, 2000.

A. Huq and et al. Ecological relationships between vibrio cholerae and planktonic crustacean copepods. *Applied and Environmental Microbiology*, 45(1):275–283, 1983.

International Organization for Migration. Population mobility tracking in haiti. Technical report, IOM, 2011. Haiti displacement and mobility data following the 2010 cholera outbreak.

L. C. Ivers and D. A. Walton. Cholera in haiti: The equity agenda and the future of global health. *The New England Journal of Medicine*, 368(3):207–209, 2013. doi: 10.1056/NEJMp1212547.

S. A. Iyaniwura, N. Ringa, P. A. Adu, S. Mak, N. Z. Janjua, M. A. Irvine, and M. Otterstatter. Understanding the impact of mobility on covid-19 spread: A hybrid gravity-metapopulation model of covid-19. *PLOS Computational Biology*, 19(2):e1011123, 2023. URL https://journals.plos.org/ploscompbiol/article?id=10.1371/journal.pcbi.1011123.

X. N. Jean-Louis. Recovering the trust of a nation: Revisiting fanon in the fight for a cholera- and gang-free haiti. *The Macksey Journal*, 1(1):1–17, 2020.

E. Jung, S. Lenhart, and Z. Feng. Optimal control of vaccination in an age-structured cholera model. *Mathematical Biosciences and Engineering*, 13(6):1241–1260, 2016.

J. M. Katz. U.s. court upholds united nations' immunity in cholera suit. *The New York Times*, 2016. URL https://www.nytimes.com/. News article.

W. O. Kermack and A. G. McKendrick. A contribution to the mathematical theory of epidemics. *Proceedings of the Royal Society A*, 115(772):700–721, 1927.

A. A. King, E. L. Ionides, M. Pascual, and M. J. Bouma. Inapparent infections and cholera dynamics. *Nature*, 454(7206):877–880, 2008.

K. Koelle, X. Rodó, M. Pascual, M. Yunus, and G. Mostafa. Refractory periods and climate forcing in cholera dynamics. *Nature*, 436(7051):696–700, 2005. doi: 10.1038/nature03821.

J. Lessler, S. M. Moore, F. J. Luquero, H. S. McKay, R. Grais, M. Henkens, and M. A. Mengel. Mapping the burden of cholera in sub-saharan africa and implications for control. *eLife*, 10:e57170, 2021. doi: 10.7554/eLife.57170.

J. Ma and D. J. D. Earn. Generality of the final size formula for an epidemic of a newly invading infectious disease. *Bulletin of Mathematical Biology*, 68(3):679–702, 2006.

L. Mari, E. Bertuzzo, L. Righetto, R. Casagrandi, M. Gatto, I. Rodriguez-Iturbe, and A. Rinaldo. Modelling cholera epidemics: the role of waterways, human mobility and sanitation. *Journal of the Royal Society Interface*, 9(67):376–388, 2012.

Z. Mukandavire, S. Liao, J. Wang, H. Gaff, D. L. Smith, and J. G. Morris. Estimating the reproductive numbers for the 2008–2009 cholera outbreaks in zimbabwe. *Proceedings of the National Academy of Sciences*, 108(21):8767–8772, 2011.

Médecins Sans Frontières. Management of a cholera epidemic, 2024. URL https://medicalguidelines.msf.org/en/viewport/CHOL/english/management-of-a-cholera-epidemic-23444438.html.

F. D. Orata, P. S. Keim, and Y. Boucher. The 2010 cholera outbreak in haiti: How science solved a controversy. *PLoS Pathogens*, 10(4), 2014. doi: 10.1371/journal.ppat.1003967. URL https://journals.plos.org/plospathogens/article?id=10.1371/journal.ppat.1003967.

A. E. Owoyemi, I. M. Sulaiman, M. Mamat, and S. E. Olowo. Stability and bifurcation analysis in a fractional-order epidemic model with sub-optimal immunity, nonlinear incidence and saturated recovery rate. *IAENG International Journal of Applied Mathematics*, 51(3), 2021.

A. E. Owoyemi, I. M. Sulaiman, P. Kumar, V. Govindaraj, and M. Mamat. Some mathematical analysis on the fractional-order 2019-ncov dynamical model. *Mathematical Methods in the Applied Sciences*, 2022. doi: 10.1002/mma.8772.

A. E. Owoyemi, C. Phang, and A. Isah. Perturbation-iteration approach for fractional-order logistic differential equations. *Nonlinear Engineering*, 14(1):20240065, 2025. doi: 10.1515/nleng-2024-0065.

Pan American Health Organization. Cholera in haiti, 2019. URL https://www.paho.org. Epidemiological summaries.

A. Pazy. *Semigroups of Linear Operators and Applications to Partial Differential Equations*, volume 44 of *Applied Mathematical Sciences*. Springer, New York, 1983.

R. Piarroux, R. Barrais, B. Faucher, R. Haus, M. Piarroux, J. Gaudart, R. Magloire, and D. Raoult. Understanding the cholera epidemic, haiti. *Emerging Infectious Diseases*, 17(7):1161–1168, 2011. doi: 10.3201/eid1707.110059.

F. Qadri, T. F. Wierzba, M. Ali, and J. D. Clemens. Cholera in the era of climate change. *The Lancet*, 402(10397):522–533, 2023. doi: 10.1016/S0140-6736(23)01058-0.

S. Rosa and D. F. M. Torres. Fractional-order modelling and optimal control of cholera transmission. *Mathematics*, 9(3):261, 2021.

H. Shu, Z. Ma, and X. Wang. Analysis of a reaction-diffusion cholera epidemic model with latent period. *Communications in Pure and Applied Analysis*, 20(6):2171–2191, 2021a.

H. Shu, Z. Ma, and X. Wang. Threshold dynamics of a nonlocal and delayed cholera model in a spatially heterogeneous environment. *Journal of Mathematical Biology*, 83(4):41, 2021b.

E. Thomas. Covid-19 modeling and final size estimates under structured risk and migration. *Universal Journal of Applied Mathematics*, 12(5):99–109, 2024. URL https://www.hrpub.org/journals/article_info.php?aid=14281.

J. H. Tien and D. J. D. Earn. Multiple transmission pathways and disease dynamics in a waterborne pathogen model. *Bulletin of Mathematical Biology*, 72(6):1506–1533, 2010. doi: 10.1007/s11538-010-9507-6.

A. R. Tuite, J. Tien, M. Eisenberg, D. J. Earn, J. Ma, and D. N. Fisman. Cholera epidemic in haiti, 2010: using a transmission model to explain spatial spread of disease and identify optimal control interventions. *Annals of Internal Medicine*, 154(9):593–601, 2011.

United Nations. World population prospects, 2022. URL https://population.un.org/wpp/. Life expectancy and demographic statistics.

P. van den Driessche and J. Watmough. Reproduction numbers and sub-threshold endemic equilibria for compartmental models of disease transmission. *Mathematical Biosciences*, 180(1):29–48, 2002.

W. Wang, Y. Zhu, R. Shen, H. Dong, and W. Wang. Effects of human mobility and behavior on disease transmission in a covid-19 metapopulation model. *Scientific Reports*, 12(1), 2022. URL https://www.nature.com/articles/s41598-022-14155-4.

F.-X. Weill, D. Domman, E. Njamkepo, A. A. Almesbahi, M. Naji, S. S. Nasher, A. Rakesh, A. M. Assiri, N. C. Sharma, I. Filliol-Toutain, and M.-L. Quilici. Cholera 2017: new challenges to an old disease. *The Lancet Infectious Diseases*, 17(11):e325–e335, 2017. doi: 10.1016/S1473-3099(17)30500-7.

World Health Organization. Cholera — haiti situation reports, 2011–2019. URL https://www.who.int/emergencies/disease-outbreak-news. Case fatality ratios and outbreak summaries.

World Health Organization. Global health observatory data repository, 2023. URL https://www.who.int/data/gho. Accessed for life expectancy and demographic estimates.

World Health Organization. Cholera outbreak toolbox, 2024. URL https://www.who.int/emergencies/outbreak-toolkit/disease-outbreak-toolboxes/cholera-outbreak-toolbox.

K. Yamazaki and X. Wang. Global stability and uniform persistence of the reaction-convection-diffusion cholera epidemic model. *Mathematical Biosciences and Engineering*, 14(2):559–579, 2017.

Y. Zhu, R. Shen, H. Dong, and W. Wang. Spatial heterogeneity and infection patterns on epidemic transmission disclosed by a combined contact-dependent dynamics and compartmental model. *PLOS ONE*, 18(6):e0286558, 2023. URL https://journals.plos.org/plosone/article?id=10.1371/journal.pone.0286558.

Appendices

Appendix A: Existence, Uniqueness, and Positivity (Bacteria)

Proof. Let's define

$$\mathbf{B}(t,x) := (B_1(t,x), B_2(t,x), B_3(t,x))^\top \Longrightarrow \tag{A.1}$$

$$\partial_t \mathbf{B}(t) = \mathcal{L}\mathbf{B}(t) + \mathcal{Q}(t)\mathbf{B}(t) + \mathbf{F}(t), \qquad t \in (0,T), \tag{A.2}$$

where $\mathcal{L}$ is the (block-diagonal) advection-diffusion operator

$$(\mathcal{L}\mathbf{B})_i = -\mathbf{v}_i \cdot \nabla B_i + D_i \Delta B_i - z_i B_i, \qquad i = 1,2,3,$$

with homogeneous Neumann boundary conditions $\nabla B_i \cdot \mathbf{n} = 0$ on $\partial\Omega$, and $\mathcal{Q}(t)$ is the (time-dependent) migration operator defined by

$$(\mathcal{Q}(t)\mathbf{B})_i = \sum_{j \neq i} q_{ji}(t)\, B_j - \sum_{j \neq i} q_{ij}(t)\, B_i, \qquad i = 1,2,3.$$

Finally, the forcing term is

$$\mathbf{F}(t,x) = \big(\tilde{\alpha} I_1(t,x) + \Lambda_1(t,x),\ \tilde{\alpha} I_2(t,x) + \Lambda_2(t,x),\ \tilde{\alpha} I_3(t,x) + \Lambda_3(t,x)\big)^\top.$$

I. Existence and Uniqueness.

For each $i = 1, 2, 3$, the operator

$$-\mathbf{v}_i \cdot \nabla + D_i \Delta - z_i$$

with homogeneous Neumann boundary conditions generates a strongly continuous (indeed analytic) semigroup on $L^2(\Omega)$. Hence, the block-diagonal operator $\mathcal{L}$ generates an analytic semigroup on $L^2(\Omega)^3$.

Moreover, since $q_{ij} \in L^\infty(0, T)$ for $i \neq j$, the operator $\mathcal{Q}(t)$ is bounded on $L^2(\Omega)^3$ for almost every $t \in (0, T)$, with

$$\|\mathcal{Q}(t)\|_{\mathcal{L}(L^2(\Omega)^3)} \leq C \max_{i \neq j} \|q_{ij}\|_{L^\infty(0,T)},$$

for some constant $C > 0$ depending only on the number of regions. In addition, the forcing term $\mathbf{F} \in L^2(0, T; L^2(\Omega)^3)$ under the stated assumptions on I_i and Λ_i.

Therefore, (A.2) is a linear nonautonomous evolution problem on $L^2(\Omega)^3$. By standard semigroup theory for linear parabolic systems (see Pazy (Pazy, 1983) and Amann (Amann, 1995)), there exists a unique mild solution satisfying

$$\mathbf{B}(t) \in C([0, T]; L^2(\Omega)^3) \cap L^2(0, T; H^1(\Omega)^3).$$

II. Positivity.

We now show the solution $\mathbf{B} = (B_1, B_2, B_3)$ constructed above remains nonnegative for all $t \in [0, T]$, provided the initial data and source terms are nonnegative.

Each equation in the system is linear and parabolic, with homogeneous Neumann boundary conditions. Moreover, the source terms satisfy

$$\tilde{\alpha} I_i(t, x) + \Lambda_i(t, x) \geq 0 \quad \text{for almost every } (t, x) \in (0, T) \times \Omega,$$

by assumption.
The coupling (migration) terms have the form

$$\sum_{j \neq i} q_{ji}(t)\, B_j - \sum_{j \neq i} q_{ij}(t)\, B_i,$$

where $q_{ij}(t) \geq 0$ for all $i \neq j$. Thus, the off-diagonal terms enter each equation with nonnegative coefficients, while the diagonal terms are non-positive. Consequently, the system is *cooperative* in the sense of monotone dynamical systems.

Equivalently, the migration operator $\mathcal{Q}(t)$ generates a positive linear operator on $L^2(\Omega)^3$; that is, if $\mathbf{B} \geq 0$ componentwise, then $\mathcal{Q}(t)\mathbf{B}$ has no negative contributions that could create sign changes. The advection-diffusion operator with Neumann boundary conditions also preserves positivity.

Therefore, the full evolution operator associated with

$$\partial_t \mathbf{B} = \mathcal{L}\mathbf{B} + \mathcal{Q}(t)\mathbf{B} + \mathbf{F}(t)$$

generates a positive semigroup on $L^2(\Omega)^3$. Since $\mathbf{B}(0) \geq 0$ and $\mathbf{F}(t) \geq 0$, standard results for cooperative parabolic systems and the weak maximum principle (see Evans (Evans, 2010)) imply

$$B_i(t,x) \geq 0 \quad \text{for almost every } x \in \Omega,\ \forall\, t \in [0,T],\ i = 1,2,3.$$

□

Appendix B: Existence, Uniqueness, and Positivity (Human)

Proof. **I. Existence of Solutions**.

Fix $i \in \{1,2,3\}$. Let

$$X_i(t) := (S_i(t), E_i(t), I_i(t), R_i(t))^\top.$$

The right-hand side of (2.1) is continuous in t and locally Lipschitz in X_i on any set where $N_i(t) = S_i + E_i + I_i + R_i$ is bounded away from 0.

Indeed, the only potentially singular term is $\frac{I_i}{N_i}$, and for nonnegative states we have $0 \leq I_i \leq N_i$, hence $\frac{I_i}{N_i} \in [0,1]$ whenever $N_i > 0$.) Therefore, by the Picard-Lindelöf theorem, for any initial condition $X_i(0) \in \mathbb{R}^4_{\geq 0}$ with $N_i(0) > 0$, there exists a unique local solution $X_i(t)$ on some interval $[0, T_{\max})$.

To extend the local solution globally, we show the total population remains bounded in time.

$$N_i(t) := S_i(t) + E_i(t) + I_i(t) + R_i(t).$$

Summing the equations in (2.1) gives

$$\frac{dN_i}{dt} = \mu - dN_i - \tilde{\nu} I_i + \Pi_i(t). \tag{B.1}$$

Since $I_i(t) \geq 0$ and $\tilde{\nu} \geq 0$, we obtain the differential inequality

$$\frac{dN_i}{dt} \leq \mu + \Pi_i(t) - dN_i. \tag{B.2}$$

Assuming $\Pi_i \in L^\infty(0,T)$ and $\Pi_i(t) \geq 0$, Grönwall's inequality (or the comparison principle for scalar ODEs) implies that for all $t \in [0,T]$,

$$0 \leq N_i(t) \leq e^{-dt} N_i(0) + \int_0^t e^{-d(t-s)} \big(\mu + \Pi_i(s)\big)\, ds \leq N_i(0) + \frac{\mu + \|\Pi_i\|_{L^\infty(0,T)}}{d}. \tag{B.3}$$

Thus $N_i(t)$ remains bounded on finite time intervals and cannot blow up in finite time.

Next we note the nonnegative orthant is forward invariant. Indeed, on the boundary where $S_i = 0$ we have

$$\frac{dS_i}{dt}\Big|_{S_i=0} = \mu + \tilde{\xi} R_i \geq 0,$$

on the boundary where $E_i = 0$ we have

$$\frac{dE_i}{dt}\Big|_{E_i=0} = \tilde{\beta} \frac{I_i}{N_i} S_i + \tilde{\eta} \frac{B_i}{K + B_i} S_i + \Pi_i(t) \geq 0,$$

on the boundary where $I_i = 0$ we have

$$\frac{dI_i}{dt}\Big|_{I_i=0} = \tilde{\sigma} E_i \geq 0,$$

and on the boundary where $R_i = 0$ we have

$$\frac{dR_i}{dt}\Big|_{R_i=0} = \tilde{\gamma} I_i \geq 0.$$

Hence $S_i(t), E_i(t), I_i(t), R_i(t)$ remain nonnegative for as long as the solution exists, and in particular $N_i(t) \geq 0$.

Finally, the bound (B.3) rules out finite-time blow-up of solutions, and therefore the local solution extends to a unique global solution on $[0, T]$ (and hence for all $t \geq 0$). This completes the proof of existence for the human SEIR subsystem.

II. Uniqueness of Solutions.

Fix $i \in \{1, 2, 3\}$ and define the state vector

$$\mathbf{X}(t) = (S_i(t), E_i(t), I_i(t), R_i(t))^\top, \qquad N_i(t) = S_i(t) + E_i(t) + I_i(t) + R_i(t).$$

Write (2.1) in the standard form

$$\frac{d\mathbf{X}}{dt} = F\big(t, \mathbf{X}\big),$$

where $F : [0, T] \times \mathbb{R}^4 \to \mathbb{R}^4$ is given by the right-hand sides of (2.1). We prove uniqueness by showing $F(t, \cdot)$ is locally Lipschitz in $\mathbf{X}$ on any positively invariant set where $N_i(t)$ is bounded away from 0.

Let $\mathcal{D} \subset \mathbb{R}^4_{\geq 0}$ be a bounded set such that

$$0 < N_{\min} \leq S + E + I + R \leq N_{\max} \quad \text{for all } (S, E, I, R) \in \mathcal{D}.$$

(Existence and positivity imply that solutions with $N_i(0) > 0$ remain in such a region on $[0, T]$.) Assume also $B_i(t) \geq 0$ and $\Pi_i(t) \geq 0$ are given bounded functions on $[0, T]$ (as ensured by the bacterial subsystem and the hypotheses on Π_i). Then the map

$$(S, E, I, R) \;\mapsto\; \frac{I}{S + E + I + R}$$

is Lipschitz on $\mathcal{D}$, since the denominator is bounded below by $N_{\min}$.

To illustrate, consider the susceptible component

$$F_S(t, \mathbf{X}) = \mu + \tilde{\xi}(1 - \epsilon_R)R - \tilde{\beta}(1 - \epsilon_S)\frac{I}{N}S - \tilde{\eta}(1 - \epsilon_B)\frac{B_i(t)}{K + B_i(t)}S - dS,$$

where $N = S + E + I + R$. Let $\mathbf{X}_1 = (S_1, E_1, I_1, R_1)$ and $\mathbf{X}_2 = (S_2, E_2, I_2, R_2)$ be in $\mathcal{D}$. Using the triangle inequality and boundedness of S and N^{-1} on $\mathcal{D}$, we obtain

$$\begin{aligned} |F_S(t, \mathbf{X}_1) - F_S(t, \mathbf{X}_2)| \leq{}& \tilde{\xi}(1 - \epsilon_R)|R_1 - R_2| + d|S_1 - S_2| \\ &+ \tilde{\beta}(1 - \epsilon_S)\left|\frac{I_1}{N_1}S_1 - \frac{I_2}{N_2}S_2\right| + \tilde{\eta}\frac{B_i(t)}{K + B_i(t)}|S_1 - S_2|. \end{aligned}$$

Moreover, since $0 \leq \dfrac{B_i(t)}{K + B_i(t)} \leq 1$, the environmental term is bounded by $\tilde{\eta}|S_1 - S_2|$.

For the incidence term, write

$$\frac{I_1}{N_1}S_1 - \frac{I_2}{N_2}S_2 = \frac{I_1}{N_1}(S_1 - S_2) + S_2\left(\frac{I_1}{N_1} - \frac{I_2}{N_2}\right).$$

On $\mathcal{D}$, $S_2 \leq N_{\max}$ and $N_1, N_2 \geq N_{\min}$, hence

$$\left|\frac{I_1}{N_1}(S_1 - S_2)\right| \leq |S_1 - S_2| \quad \text{and} \quad \left|\frac{I_1}{N_1} - \frac{I_2}{N_2}\right| = \left|\frac{I_1N_2 - I_2N_1}{N_1N_2}\right| \leq \frac{1}{N_{\min}^2}\Big(|I_1 - I_2|\, N_{\max} + |N_1 - N_2|\, N_{\max}\Big).$$

Since $|N_1 - N_2| \leq |S_1 - S_2| + |E_1 - E_2| + |I_1 - I_2| + |R_1 - R_2|$, it follows:

$$\left|\frac{I_1}{N_1}S_1 - \frac{I_2}{N_2}S_2\right| \leq C\Big(|S_1 - S_2| + |E_1 - E_2| + |I_1 - I_2| + |R_1 - R_2|\Big),$$

for a constant $C > 0$ depending only on $N_{\min}$ and $N_{\max}$. Therefore, for each fixed $t \in [0, T]$,

$$|F_S(t, \mathbf{X}_1) - F_S(t, \mathbf{X}_2)| \leq L\|\mathbf{X}_1 - \mathbf{X}_2\|$$

for some constant $L > 0$ independent of $\mathbf{X}_1, \mathbf{X}_2 \in \mathcal{D}$.

The same argument applies to $F_E(t, \mathbf{X})$, since it contains the same incidence terms and otherwise only linear terms, while F_I and F_R are linear in (E, I, R). Hence $F(t, \cdot)$ is locally Lipschitz on $\mathcal{D}$ uniformly in $t \in [0, T]$. By the Picard-Lindelöf theorem, solutions to (2.1) with the same initial data are unique on $[0, T]$.

III. Positivity of Solutions.

We now show solutions of the human SEIR system (2.1) remain nonnegative for all $t \geq 0$, provided they start from nonnegative initial data. Assume

$$S_i(0) \geq 0, \qquad E_i(0) \geq 0, \qquad I_i(0) \geq 0, \qquad R_i(0) \geq 0,$$

with $N_i(0) > 0$.

We verify the nonnegative orthant $\mathbb{R}^4_{\geq 0}$ is forward invariant by examining the vector field on each coordinate hyperplane.

- **Susceptible compartment.** If $S_i = 0$, then

$$\frac{dS_i}{dt}\Big|_{S_i=0} = \mu + \tilde{\xi}(1 - \epsilon_R)R_i \geq 0,$$

  since $\mu \geq 0$ and $R_i \geq 0$.
- **Exposed compartment.** If $E_i = 0$, then

$$\frac{dE_i}{dt}\Big|_{E_i=0} = \tilde{\beta}(1 - \epsilon_S)\frac{I_i}{N_i}S_i + \tilde{\eta}(1 - \epsilon_B)\frac{B_i}{K + B_i}S_i + \Pi_i(t) \geq 0,$$

  because $S_i, I_i, B_i, \Pi_i(t) \geq 0$.

- **Infectious compartment.** If $I_i = 0$, then

$$\frac{dI_i}{dt}\Big|_{I_i=0} = \tilde{\sigma}(1-\epsilon_E)E_i \geq 0,$$

since $E_i \geq 0$.

- **Recovered compartment.** If $R_i = 0$, then

$$\frac{dR_i}{dt}\Big|_{R_i=0} = \gamma(1+\epsilon_I)I_i \geq 0,$$

since $I_i \geq 0$.

Thus, on each boundary face of the nonnegative orthant, the vector field points inward or is tangent. Consequently, no component of the solution can cross into negative values. Therefore,

$$S_i(t) \geq 0, \quad E_i(t) \geq 0, \quad I_i(t) \geq 0, \quad R_i(t) \geq 0 \qquad \text{for all } t \geq 0.$$

This shows the human SEIR subsystem preserves positivity.

Since existence, uniqueness, and positivity have been established, the human population subsystem is well posed.

□

Appendix C: Lyapunov Stability Derivations

Proof. We consider the infected and environmental subsystems of the three-region SEIR-B model. Assume there is *no exogenous contamination*, i.e.

$$\Lambda_i(t) \equiv 0, \qquad i = 1, 2, 3.$$

Note: Only Region 1 has waterway outflow to Region 2 through $q_{12}(t)$, and Region 3 receives infection pressure through migration terms $m_{13}I_1$ and $m_{23}I_2$ entering E_3.

Let is define

$$L(t) = a\,(E_1^2 + E_2^2 + E_3^2) + b\,(I_1^2 + I_2^2 + I_3^2) + c_1B_1^2 + c_2B_2^2 + c_3B_3^2, \tag{C.1}$$

where $a, b, c_1, c_2, c_3 > 0$. Then $L(t) > 0$ for all nonzero states and $L(t) = 0$ only at the disease-free state in the (E, I, B) variables.

Differentiating (C.1) gives

$$\dot{L}(t) = 2a\sum_{i=1}^{3} E_i\dot{E}_i + 2b\sum_{i=1}^{3} I_i\dot{I}_i + 2c_1B_1\dot{B}_1 + 2c_2B_2\dot{B}_2 + 2c_3B_3\dot{B}_3.$$

Using Young's inequality and recognizing that $\frac{B_i}{K+B_i} \leq \frac{B_i}{K}$ and $S_i \leq N_i \leq \frac{\mu}{d}$ and $\frac{S_i}{N_i} < 1$, we can rewrite $\frac{dL}{dt}$ as the following inequality:

$$
\begin{aligned}
\frac{dL}{dt} \leq\ & \left(2Ka\beta\mu - 2Ka\,d^2 - 2Kad\sigma + 2Kbd\sigma + 2a\eta\mu\right) E_1^2 \\
& + \left(2Ka\beta\mu - 2Ka\,d^2 - 2Kad\sigma + 2Kbd\sigma + 2a\eta\mu\right) E_2^2 \\
& + \left(2Ka\beta\mu - 2Ka\,d^2 + 2Kadm_{13} + 2Kadm_{23} - 2Kad\sigma + 2Kbd\sigma + 2a\eta\mu\right) E_3^2 \\
& - 2dK\left(-am_{13} - \alpha c_1 + bd + b\gamma + b\nu - b\sigma\right) I_1^2 \\
& - 2dK\left(-am_{23} - \alpha c_2 + bd + b\gamma + b\nu - b\sigma\right) I_2^2 \\
& - 2dK\left(-\alpha c_3 + bd + b\gamma + b\nu - b\sigma\right) I_3^2 \\
& + \left(2K\alpha c_1 d - 2Kc_1 dq_{12} - 2Kc_1 dz1 + 2Kc_2 dq_{12} + 2a\eta\mu\right) B_1^2 \\
& + \left(2K\alpha c_2 d + 2Kc_2 dq_{12} - 2Kc_2 dz2 + 2a\eta\mu\right) B_2^2 \\
& + \left(2K\alpha c_3 d - 2Kc_3 dz3 + 2a\eta\mu\right) B_3^2
\end{aligned}
$$

Let us define the following coefficients:

$$
a = R_H = \frac{\beta\sigma}{(\sigma+d)(d+\gamma+\nu)}; \quad b = \frac{1}{\gamma+\nu+d}; \quad c_1 = \frac{1}{q_{12}+z_1}; \quad c_2 = \frac{1}{z_2}; \quad c_3 = \frac{1}{z_3};
$$

When $\mathcal{R}_0 < 1 \Longrightarrow \mathcal{R}_H < 1$ thereby making all of the coefficients before the E_i^2, I_i^2, and B_i^2 terms negative. Thus, $\dot{L} \leq 0$, therefore, by LaSalle's Invariance Principle the DFE is globally asymptotically stable whenever $\mathcal{R}_0 < 1$. □

Appendix D: Final Epidemic Size

Proof. We begin with the susceptible equation in region i:

$$
\frac{dS_i}{dt} = \mu + \tilde{\xi}R_i - \tilde{\beta}\frac{I_i}{N_i}S_i - \tilde{\lambda}\frac{B_i}{K+B_i}S_i - dS_i.
$$

Following the classical final-size derivations (Hethcote, 2000; Diekmann et al., 2013; Ma and Earn, 2006; Brauer et al., 2019), we consider a single epidemic wave on a time window $[0, T]$ and assume, over this window, demographic turnover and other slow processes (births, natural deaths, waning immunity, reinfection terms, and migration) contribute negligibly compared to the infection process. Under this epidemic-time-scale approximation,

$$
\frac{dS_i}{dt} \approx -\left(\tilde{\beta}\frac{I_i(t)}{N_i(t)} + \tilde{\lambda}\frac{B_i(t)}{K+B_i(t)}\right) S_i(t) \Longrightarrow \tag{D.1}
$$

$$
\int_{S_i(0)}^{S_i(T)} \frac{dS_i}{S_i} = -\int_0^T \left(\tilde{\beta}\frac{I_i(t)}{N_i(t)} + \tilde{\lambda}\frac{B_i(t)}{K+B_i(t)}\right) dt, \Longrightarrow \tag{D.2}
$$

$$
\ln\left(\frac{S_i(T)}{S_i(0)}\right) = -\tilde{\beta}\int_0^T \frac{I_i(t)}{N_i(t)}\,dt - \tilde{\lambda}\int_0^T \frac{B_i(t)}{K+B_i(t)}\,dt. \tag{D.3}
$$

Define the final susceptible fraction (final size variable)

$$
u_i := \frac{S_i(T)}{S_i(0)} \in (0, 1],
$$

and the cumulative infection pressures

$$\mathcal{H}_i := \tilde{\beta} \int_0^T \frac{I_i(t)}{N_i(t)}\, dt, \qquad \mathcal{E}_i := \tilde{\lambda} \int_0^T \frac{B_i(t)}{K + B_i(t)}\, dt.$$

Then the final size identity becomes the exact relation

$$\ln\left(\frac{1}{u_i}\right) = \mathcal{H}_i + \mathcal{E}_i. \tag{D.4}$$

The quantity $\mathcal{H}_i$ represents the *cumulative human-to-human infection pressure* experienced by susceptibles in Region i over the interval $[0, T]$, while $\mathcal{E}_i$ denotes the *cumulative environmental infection pressure* arising from exposure to contaminated water over the same period. Equation (D.4) therefore states that the logarithmic depletion of susceptibles equals the total accumulated force of infection, human and environmental, during a single epidemic wave.

If, in addition, the total population size remains approximately constant ($N_i(t) \approx N_i(0)$ on $[0, T]$) and the epidemic wave is driven by endogenous transmission characterized by $\mathcal{R}_0$, then (D.4) reduces to the familiar attack-rate form

$$\ln\left(\frac{1}{u_i}\right) = \mathcal{R}_0\,(1 - u_i) + \mathcal{E}_i,$$

where $1 - u_i$ is the fraction infected during the outbreak and $\mathcal{E}_i$ captures the additional contribution of environmental exposure. In the absence of environmental transmission ($\mathcal{E}_i = 0$), this expression recovers the classical final size relation $\ln(\frac{1}{u_i}) = \mathcal{R}_0(1 - u_i)$.

□

Appendix E: Global Stability of the Bacteria-Free State

Proof. We consider the bacterial concentration $B_i(t, x)$ in region $i \in \{1, 2, 3\}$ governed by the transport-diffusion equation

$$\frac{\partial B_i}{\partial t} + \mathbf{v}_i \cdot \nabla B_i = D_i \nabla^2 B_i + \tilde{\alpha}\, I_i + \sum_{j \neq i} q_{ji}(t)\, B_j - \sum_{j \neq i} q_{ij}(t)\, B_i - z_i B_i + \Lambda_i(t),$$

subject to nonnegative initial data $B_i(0, x) \geq 0$.

We analyze the global stability of the bacteria-free equilibrium

$$B_i^*(x) \equiv 0, \qquad i \in \{1, 2, 3\}.$$

Assume the infectious populations $I_i(t, x)$ and external inputs $\Lambda_i(t)$ are uniformly bounded, so that

$$0 \leq I_i(t, x) \leq I_{\max}, \qquad 0 \leq \Lambda_i(t) \leq \Lambda_{\max},$$

for all $t \geq 0$ and $x \in \Omega$.

Define the Lyapunov functional

$$L(t) := \frac{1}{2}\sum_{i=1}^{3}\int_{\Omega} B_i(t,x)^2\,dx.$$

Clearly, $L(t) \geq 0$ with equality if and only if $B_i(t,x) \equiv 0$ for all i. Differentiating $L(t)$ along solutions gives

$$\begin{aligned}\frac{dL}{dt} &= \sum_{i=1}^{3}\int_{\Omega} B_i \frac{\partial B_i}{\partial t}\,dx \\ &= \sum_{i=1}^{3}\int_{\Omega} B_i\Big(D_i\nabla^2 B_i - \mathbf{v}_i\cdot\nabla B_i + \tilde{\alpha}I_i + \sum_{j\neq i} q_{ji}(t)B_j - \sum_{j\neq i} q_{ij}(t)B_i - z_i B_i + \Lambda_i(t)\Big)\,dx.\end{aligned}$$

We impose homogeneous Neumann boundary conditions $\partial B_i/\partial n = 0$ on $\partial\Omega$ and assume $\mathbf{v}_i\cdot\mathbf{n} = 0$ on $\partial\Omega$ with $\nabla\cdot\mathbf{v}_i = 0$. Then, by Green's identity and the divergence theorem,

$$\int_{\Omega} B_i\nabla^2 B_i\,dx = -\int_{\Omega}|\nabla B_i|^2\,dx, \qquad \int_{\Omega} B_i\,\mathbf{v}_i\cdot\nabla B_i\,dx = 0.$$

Substituting these identities yields

$$\begin{aligned}\frac{dL}{dt} = &-\sum_{i=1}^{3} D_i\int_{\Omega}|\nabla B_i|^2\,dx - \sum_{i=1}^{3} z_i\int_{\Omega} B_i^2\,dx - \sum_{i=1}^{3}\sum_{j\neq i}\int_{\Omega} q_{ij}(t)B_i^2\,dx \\ &+\sum_{i=1}^{3}\sum_{j\neq i}\int_{\Omega} q_{ji}(t)B_iB_j\,dx + \sum_{i=1}^{3}\int_{\Omega} B_i\big(\tilde{\alpha}I_i + \Lambda_i(t)\big)\,dx.\end{aligned}$$

The transport terms represent redistribution between regions. Using the inequality $B_iB_j \leq \frac{1}{2}(B_i^2 + B_j^2)$ and assuming uniform lower bounds $\underline{q}_{ij}$ on the outflow rates $q_{ij}(t)$, we obtain

$$\sum_{i,j\neq i}\int_{\Omega} q_{ji}(t)B_iB_j\,dx \;\leq\; \sum_{i=1}^{3}\sum_{j\neq i}\underline{q}_{ij}\int_{\Omega} B_i^2\,dx.$$

Consequently,

$$\frac{dL}{dt} \leq -\sum_{i=1}^{3}\left(z_i + \sum_{j\neq i}\underline{q}_{ij}\right)\int_{\Omega} B_i^2\,dx + \sum_{i=1}^{3}\int_{\Omega} B_i\big(\tilde{\alpha}I_{\max} + \Lambda_{\max}\big)\,dx.$$

Applying Young's inequality to the source terms and defining the bacterial reproduction threshold

$$\mathcal{Q}_B := \max_{i\in\{1,2,3\}}\frac{\tilde{\alpha}I_{\max} + \Lambda_{\max}}{z_i + \sum_{j\neq i}\underline{q}_{ij}},$$

we conclude

$$\frac{dL}{dt} \leq -C\, L(t) \quad \text{whenever} \quad \mathcal{Q}_B < 1,$$

for some constant $C > 0$. Therefore, $L(t) \to 0$ as $t \to \infty$, which implies

$$B_i(t, x) \to 0 \quad \text{for all } i \in \{1, 2, 3\} \text{ and } x \in \Omega.$$

Hence, the bacteria-free equilibrium is globally asymptotically stable whenever $\mathcal{Q}_B < 1$. □

Appendix F: Monotonicity of Environmental Contamination

Proof. We consider the bacterial concentration in region i, governed by

$$\frac{\partial B_i}{\partial t} + \mathbf{v}_i \cdot \nabla B_i = D_i \nabla^2 B_i + \tilde{\alpha}\, I_i + \sum_{j \neq i} q_{ji}(t)\, B_j - \sum_{j \neq i} q_{ij}(t)\, B_i - z_i B_i + \Lambda_i(t). \tag{F.1}$$

We assume zero–flux boundary conditions and either spatial homogeneity or consider the spatial average over a bounded domain Ω. Define the spatial mean

$$\bar{B}_i(t) := \frac{1}{|\Omega|} \int_\Omega B_i(t, x)\, dx.$$

Under these assumptions, the diffusion and advection terms vanish upon integration, yielding the reduced mean–field equation

$$\frac{d\bar{B}_i}{dt} = \tilde{\alpha}\, \bar{I}_i + \sum_{j \neq i} \bar{q}_{ji}\, \bar{B}_j - \sum_{j \neq i} \bar{q}_{ij}\, \bar{B}_i - z_i \bar{B}_i + \bar{\Lambda}_i, \tag{F.2}$$

where bars denote time–averaged quantities and all coefficients are nonnegative.

Fix all parameters except $\bar{\Lambda}_i$. At equilibrium,

$$0 = \tilde{\alpha}\, \bar{I}_i + \sum_{j \neq i} \bar{q}_{ji}\, \bar{B}_j^* - \sum_{j \neq i} \bar{q}_{ij}\, \bar{B}_i^* - z_i \bar{B}_i^* + \bar{\Lambda}_i.$$

Rearranging gives

$$\bar{B}_i^* = \frac{\tilde{\alpha}\, \bar{I}_i + \sum_{j \neq i} \bar{q}_{ji}\, \bar{B}_j^* + \bar{\Lambda}_i}{z_i + \sum_{j \neq i} \bar{q}_{ij}}.$$

The denominator is strictly positive. Differentiating implicitly with respect to $\bar{\Lambda}_i$ yields

$$\frac{\partial \bar{B}_i^*}{\partial \bar{\Lambda}_i} = \frac{1}{z_i + \sum_{j \neq i} \bar{q}_{ij}} \; > \; 0.$$

Thus, the equilibrium bacterial concentration in region i depends *strictly monotonically* on the exogenous environmental input $\bar{\Lambda}_i$. In particular, if $\bar{\Lambda}_i^{(2)} > \bar{\Lambda}_i^{(1)}$, then

$$\bar{B}_i^*(\bar{\Lambda}_i^{(2)}) > \bar{B}_i^*(\bar{\Lambda}_i^{(1)}).$$

Finally, if $\bar{I}_i = 0$ and $\bar{\Lambda}_i > 0$, then

$$\bar{B}_i^* = \frac{\bar{\Lambda}_i}{z_i + \sum_{j \neq i} \bar{q}_{ij}} > 0,$$

so a strictly positive environmental equilibrium persists even in the absence of local human infection. If $\bar{I}_i = 0$ and $\bar{\Lambda}_i = 0$, then $\bar{B}_i^* = 0$ is the unique equilibrium. This establishes monotone dependence of the environmental bacterial equilibrium on exogenous contamination and completes the proof. □